Russian Journal of Earth Sciences

Earthquake Loss Simulation Using the "Extremum" System: An Example of Morocco's Territory

N. I. Frolova[*,1], J. A. Peláez[2], M. Hamdache[3], A. Kijko[4], S. P. Sushchev[5], and N. S. Malaeva[1,6]

[1]Sergeev Institute of Environmental Geosciences, Russian Academy of Sciences, Moscow, Russia
[2]Department of Physics, University of Jaén, Jaén, Spain
[3]Seismic Division, CRAAG, Algiers, Algeria
[4]Natural Hazard Centre, University of Pretoria, Pretoria, South Africa
[5]Bauman Moscow State Technical University, Moscow, Russia
[6]FSBE All-Russian Research Institute for Civil Defence of the EMERCOM of Russia (the Federal Science and High Technology Center), Moscow, Russia
* **Correspondence to:** Nina Frolova, frolovanina7@gmail.com

Abstract: The study describes the use of the Extremum system for simulating near-real-time effects related to the devastating earthquake that struck Morocco on September 8, 2023, as well as the consequences of several scenario events for potentially hazardous source zones in the High Atlas (HA) region. The study's relevance stems from the need for accurate estimates of potential losses resulting from recent earthquakes to support response decision-making and potential scenario events in the most hazardous zones, as well as to create and conduct early action plans to reduce seismic risk. The calibration of the seismic intensity attenuation models for the Moroccan area using the Extremum system is the aim of this work, too, to investigate the applicability of seismic intensity attenuation equations previously established, for near-real-time loss assessment for strong events and scenario events that could occur in the study area. It is worth pointing out that our work is the first to analyze these equations. We also look into the impact of regional vulnerability functions on typical building stock and earthquake loss simulation outcomes. The study presents the results of a potential source zone identification based on an established catalog. Considering the weighted value, three distinct procedures are employed to calculate the maximum possible magnitudes for these zones. In this context, a comparison of the projected effects for the cities of Targua and Adassil, located in the severely devastated province of Chichaoua, demonstrates a satisfactory match between the observed and expected damage to the infrastructure.

Keywords: Near real-time earthquake loss estimation, scenario events, source zones, Extremum information system, calibration of macroseismic field models, Morocco.

Citation: Frolova N. I., Peláez J. A., Hamdache M., Kijko A., Sushchev S. P., and Malaeva N. S. (2025), Earthquake Loss Simulation Using the "Extremum" System: An Example of Morocco's Territory, *Russian Journal of Earth Sciences*, 25, ES6024, EDN: ZOKFVP, https://doi.org/10.2205/2025es001069

Research Article

Received: January 23, 2025
Accepted: June 23, 2025
Published: December 30, 2025

1. Introduction

According to statistics from the International Center for the Epidemiology of Disasters (EMDAT), the number of deaths from earthquakes in 2023 exceeded 60,000, double the average annual estimates from the period 2003 to 2022. The February 6 earthquakes in Turkey and Syria, September 8 in Morocco, and October 7, 11, and 15 earthquakes in Afghanistan were among the ten most severe natural disasters of 2023 in fatalities. All three catastrophic events took place in the Alpine-Himalayan seismic belt.

The tragic consequences of the 2023 earthquakes demonstrate that despite significant progress in the study of catastrophic earthquakes worldwide and improvements in regulations for earthquake-resistant construction, these earthquakes remain unpredictable, and seismic risk remains high. The issues of ensuring the safety of the population and territories from seismic disasters and related secondary hazards remain highly relevant.

The Commission on Data of the International Science Council, CODATA, statement dated March 1, 2023 (http://www.codata.org/), regarding the tragedy in Turkey and Syria, notes the importance of scientific efforts in providing timely information for decision-makers on rescue and other urgent actions, and also for rendering humanitarian assistance. Global near-real-time systems can provide information for loss assessment, having been successfully developed over the past 20 years and actively using big data to calibrate their models. Currently, at least three systems, DGACS, Extremum, and PAGER, provide information on the possible consequences of strong events in emergency mode.

The Coordination System (GDACS) is designed to monitor the seismic situation in near real-time and evaluate the estimated number of residents likely living in the affected area based on population density data (https://gdacs.org/) [*De Groeve*, 2007; *De Groeve et al.*, 2008].

The Extremum System [*Frolova et al.*, 2017, 2014; *Kagan*, 2002b; *Larionov and Frolova*, 2003] can simulate the distribution of shaking intensity, the damage to various types of buildings, the number of casualties in damaged and destroyed structures, and, optionally, identify effective response measures needed in case of an emergency.

Finally, the Prompt Assessment of Global Earthquakes for Response (PAGER) system, developed by the US Geological Survey, allows for the simulation of expected shaking intensity and estimating the number of residents in zones of different intensities based on population density information.

It should be noted that the Global Earthquake Model (GEM), which a public-private partnership initiated by the Global Science Forum of the Organisation for Economic Co-operation and Development, is developing a similar system (https://www.globalquakemodel.org). They developed and actively promote the OpenQuake-engine for seismic hazard and risk calculations [*The OpenQuake-engine User Manual. Global Earthquake Model (GEM) Open-Quake Manual for Engine version 3.0.0*, 2018]. The GEM team has recently presented Real-Time Loss Tools, based on OpenQuake-engine software, that allow to estimate damage and loss due to earthquake sequences accounting for damage accumulation and the displacement of the building occupants. In the publication [*Nievas et al.*, 2025] they gave the example of the retrospective damage and loss due to the 2023 Türkiye-Syria Sequence events.

In this investigation, the Extremum system is used.

The first version of Extremum was developed in the 1990s and first tested during the 1995 M_w = 7.1 Neftegorsk earthquake on Sakhalin Island, Russia [*Frolova et al.*, 2017]. In the 2000s, under the Council of Europe Partial Agreement on Major Hazards, programs STRIM and EDRIM fostered a version of the Extremum system to assess global earthquake losses.

The experience gained from applying Extremum allowed for ranking factors responsible for earthquake effects. Four factors were identified: a) source, b) macroseismic field, c) building vulnerability, and d) population vulnerability. The primary contribution to the uncertainty in near-real-time simulation arises from errors in determining the earthquake's location coordinates, source depth, magnitude, and source mechanism, particularly the orientation of the source rupture and predicted seismic intensity. The results of extensive research and experience, based on processing numerous strong earthquakes globally, facilitated the development of an efficient procedure for calibrating the macroseismic field and identifying zones with "quasi-stable" parameters, such as the regional coefficients of seismic intensity attenuation models, along with the orientation and shape of the isoseismals.

The primary focus of this study is the M_w = 6.8 Moroccan earthquake that occurred on September 8, 2023. This event calibrates the Extremum and applies it to loss simulation across various seismogenic zones. Several seismic intensity attenuation models for Morocco and its surrounding regions were evaluated. The best agreement between the simulated and observed damages was found for the models developed specifically for the High Atlas (HA) and Middle Atlas (MA) zone [*Cherkaoui*, 1991], Algeria, the Atlas Mountains [*Benouar*,

1994], and the territory of Turkey [*Aliaj*, 1982]. A comparison of the simulated impacts for the municipalities of Adassil and Targua in the heavily affected province of Chichaoua, Morocco, showed satisfactory alignment between the expected and observed infrastructure damage. The calibrated Extremum models simulated damages from potential future events in the High Atlas zone. These results can inform the development and implementation of preventive measures to reduce the negative impacts of future earthquakes. Although earthquake-like events in the Atlas region are rare, this is history's most decisive recorded event. It has been selected as the focus of our research to calibrate the Extremum system for northwestern Africa.

2. Seismotectonic Sketch of the Study Region

The seismicity of the African continent has been the subject of several studies, with the earliest dating back to the beginning of the twentieth century. One of the initial studies dedicated to the seismicity of the African continent and the identification of seismotectonic zones was conducted as part of the UNESCO Project [*Gorshkov*, 1963a,b]. Subsequently, a project titled "Seismotectonic and Seismic Hazard in Africa" was supported by UNESCO-Paris (Project 601) and UNESCO-Nairobi from 2011 to 2016 [*Meghraoui and the IGBP-601 working group*, 2016]. It is important to note that multiple studies have focused on this topic, including those by [*Skobelev et al.*, 2004], [*Craig et al.*, 2011], and [*Letamo et al.*, 2023].

The area in which the studied earthquake occurred, northern Morocco, is located at the boundary between the Nubian and Eurasian Plates, and it is a complex region from a tectonic point of view (Fig. 1). The direct contact among these two plates in this region, with a convergence rate of approximately 4 mm/year [*DeMets et al.*, 2010], can be divided into two sectors [*Peláez et al.*, 2018a], a) that situated from the Azores Islands, i.e., the Middle Atlantic Ridge, to the Strait of Gibraltar (the so-called the Azores-Gibraltar transform zone), and b) the Alboran Sea region.

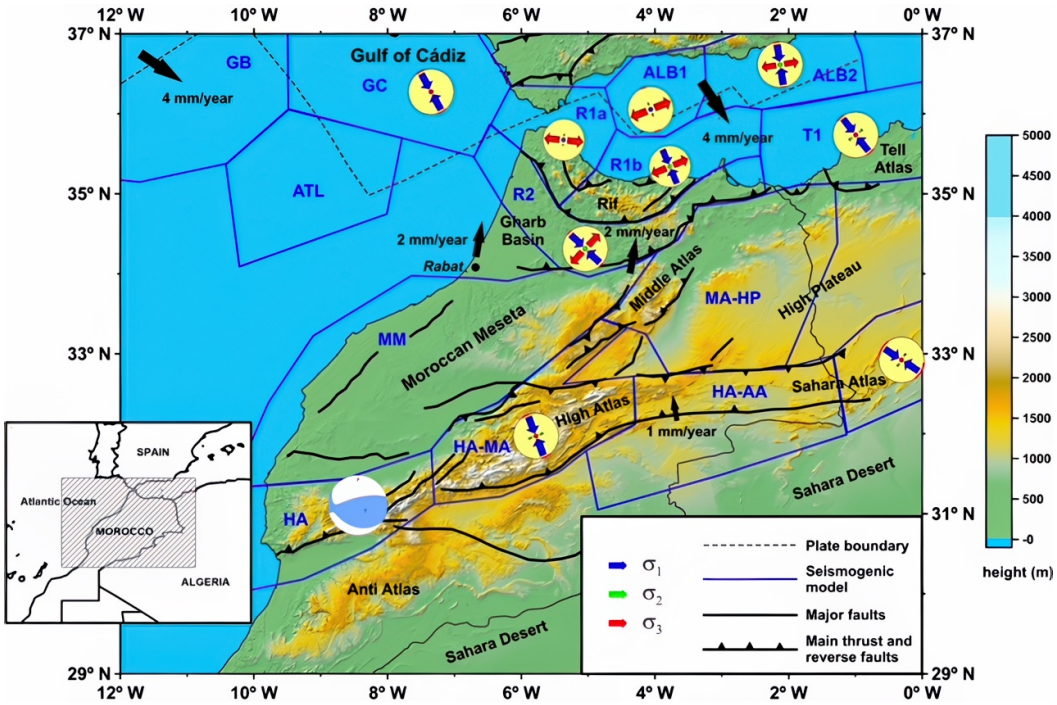

Figure 1. Simplified tectonic map of Morocco after [*Peláez et al.*, 2007] including the seismogenic model by [*Peláez et al.*, 2018a,b]. Main tectonic domains are depicted, including plate boundaries [*Hasterok et al.*, 2022], known convergence rates [*Chalouan et al.*, 2023; *DeMets et al.*, 2010], and computed minimum (SH_{min}) and maximum (SH_{max}) local horizontal stress axes [*Peláez et al.*, 2018a,b]. The USGS provided the focal mechanisms for the 2023 earthquake.

The Azores-Gibraltar transform zone is well-defined in its western and central sections. In the eastern section, the continuity of the faults is not well known. All that is currently known is that they are poorly marked, striking E–W faults. This contributes to establishing a diffuse plate border [*Rosas et al.*, 2012]. Only the eastern end of this region, the Gulf of Cadiz, is considered here.

The second sector, the Alboran Sea, located at the western end of the Mediterranean Sea, features a thinned continental crust between the Rif in Morocco and the Betic Cordillera in Spain. This thin continental crust results from a less intense opening process of the Algero-Provençal basin; in fact, the Alboran Sea is the western extension of this basin. Concurrent with this process is the formation of the Strait of Gibraltar, which delineates an arc [*López Casado et al.*, 2001] or represents a pure subduction process [*Pedrera et al.*, 2011].

The effects generated by the convergence of the Nubia and Eurasian Plates are not limited to the Azores-Gibraltar transform zone and the Alboran Sea. This convergence also propagates to the south [*Chalouan et al.*, 2023], developing the Rif and Tell Cordilleras along the northern Moroccan and Algerian coasts, and more to the south, the Atlas Mountains or Atlas Belt (Middle Atlas to the north and High Atlas to the south and southwest), going from the northeast to the southwest of Morocco (Fig. 1). The Moroccan Meseta (MM), formed by Paleozoic rocks between the Rif and the Atlas, is also affected. In the western section of the High Atlas, where the 2023 event occurred, diverse striking NE–SW faults [*Mridekh*, 2002; *Sébrier et al.*, 2006] can be observed. The computed shortening in the eastern section of the High Atlas [*Chalouan et al.*, 2023], which is also expected to occur in its western section, suggests the presence of active reverse or strike-slip faults, many of which remain unidentified today. These faults were active during the Mio-Pliocene and the Quaternary [*Ait Brahim et al.*, 2002; *Sébrier et al.*, 2006].

A previous study [*Peláez et al.*, 2018a,b] demonstrated the stress pattern computed for this region based on available focal mechanism solutions. This pattern was derived using the inversion technique developed by [*Delvaux and Sperner*, 2003] with the assistance of Win-Tensor software. Results, consistent with the tectonic framework of the Ibero-Maghrebian region and the study by [*Henares et al.*, 2003], are presented in Fig. 1. In the Gulf of Cadiz and Tell, a clear strike-slip compressional NW–SE to NNW–SSE regime is observed, with σ_1 and σ_2 nearly horizontal, combined with a perpendicular extension in the Rif and northeastern Alboran Sea region, where σ_1 and σ_3 are roughly horizontal [*Vázquez et al.*, 2022]. In the central section, the Strait of Gibraltar area and the northwestern section of the Alboran Sea, the prevailing stress is an EW to ESE–WNW extension combined with a near-vertical compression. The High Atlas, the only southern region with available data, showed a similar stress pattern to that of the Gulf of Cadiz and Tell regions, a strike-slip compressional NNW–SSE regime. In a more recent work, [*Sparacino et al.*, 2020] obtained similar results for the region's northern part from GNSS data from several local and regional geodetic networks. A NW–SE shortening of 12 nano strain/year and a NE–SW elongation of 16 nano strain/year were computed in southern Spain's eastern Rif, mostly Alboran Sea, and Betic Cordilleras. In addition, high values were obtained for the seismic coupling coefficient (percentage of the seismic and geodetic moment-rate ratio) in the Rif and central and eastern High Atlas zones. No conclusive (poorly constrained) results were obtained for the western High Atlas zone, where the 2023 earthquake was located.

The largest earthquakes and the most significant seismicity rate in this region are observed (Fig. 2) along the Azores-Gibraltar transform zone, also including nearby areas, that is, the Rif in northern Morocco, the Tell in northwestern Algeria, and the Betic Cordillera in southern Spain [*Peláez et al.*, 2007]. Earthquakes located along the Atlas are fewer in number, although not unusual. Finally, seismicity in the Moroccan Meseta, Anti-Atlas and High Plateau is scarce, except for some seismic sequences.

In recent decades, the most significant and damaging earthquakes impacting Morocco were the Al-Hoceima earthquakes of 1994, 2004, and 2016 [*Hamdache et al.*, 2022], which occurred both onshore and offshore in the Rif, the most seismically active area in Morocco

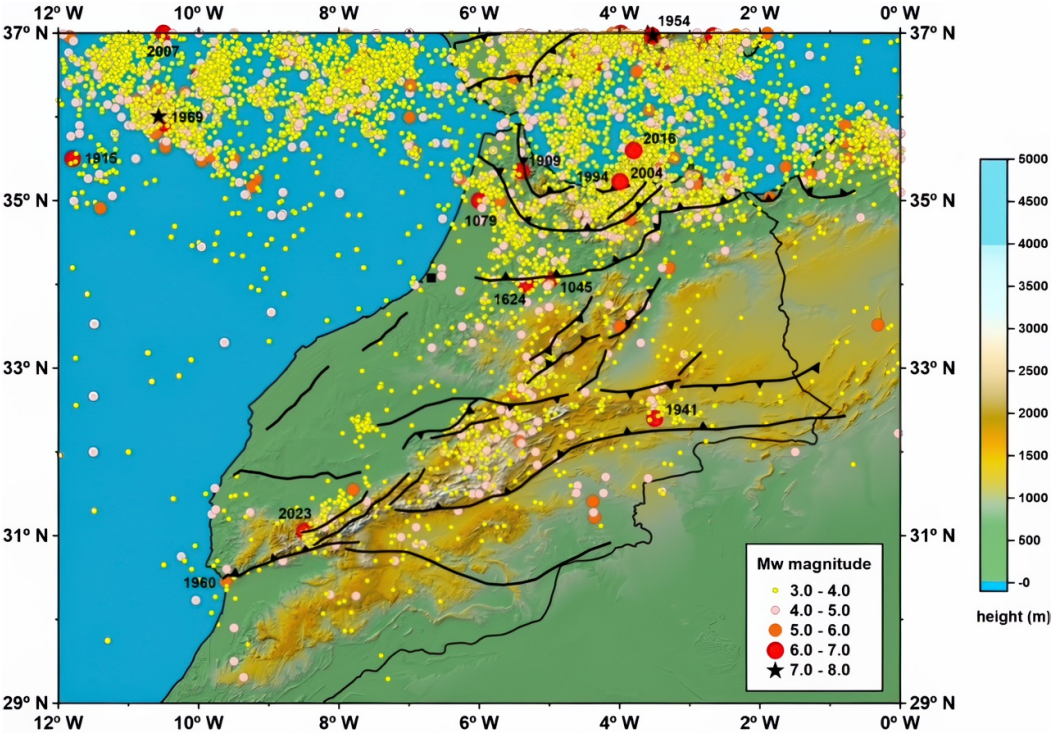

Figure 2. Seismicity from the Spanish IGN seismic catalog, completed with the catalog by *Peláez et al.* [2007]. The most significant events are highlighted.

and the western Mediterranean region. Their magnitudes ranged from M_w = 6.0 to 6.4. The 2004 M_w = 6.4 event resulted in over 600 deaths and 15,000 homeless, causing extensive damage. According to [*Kariche et al.*, 2018], this event occurred on a NE–SW strike-slip fault, although NW–SE faults with conjugate branches have also been suggested as the source of this earthquake [*van der Woerd et al.*, 2014].

The February 1960 M_w = 5.9 Agadir earthquake [*AISE*, 1962] remains vivid in the memory of the Moroccan people. It was situated on the boundary between the western High Atlas and the Anti-Atlas (AA) (Fig. 2). This event had a precedent in the same region, with the 1731 earthquake, which had a similar or greater magnitude based on the felt intensity [*Peláez et al.*, 2007]. In the Agadir earthquake, between 12,000 and 15,000 people lost their lives, representing one-third of Agadir's population, necessitating the city to be almost wholly rebuilt afterward. To the south of Morocco, in the eastern section of the High Atlas, near the town of Talsint, an earthquake with intensity VIII was recorded in June 1941.

Other significant earthquakes took place in the historical period. For instance, the 1709 earthquake, felt with intensity IX (M_w = 6.6 macroseismic magnitude), and the January 1909 earthquake (m_b = 5.8 in [*Cherkaoui*, 1988] and m_b = 6.2 in the CNRST catalogue), both located in the Rif. Also, the 1045 and 1624 earthquakes are located in Fez, in the Rif and the Moroccan Meseta boundary, with felt Intensities equal to VIII and IX–X, respectively.

Some significant earthquakes have also occurred in the Gulf of Cadiz area. However, given the distance to Moroccan territory, they are not the main contributors to the Moroccan seismic hazard and risk, although they were felt. During the instrumental epoch, 1915, 1969, and 2007 events stand out. The July 1915 M_w = 6.2 event, recorded by the Spanish IGN network, was felt with intensity V along the Portuguese coast, but no data on Morocco is provided. The February 1969 M_w = 7.8 earthquake was the largest event recorded in this region, with an intensity of VII felt along the Portuguese coast and intensity VI extensively along the Moroccan coast [*Mezcua*, 1982]. Finally, in February 2007, a M_w = 6.1 earthquake was recorded at a depth of 65 km and felt with intensity IV along the Spanish Gulf of Cadiz coast, with no data available for the Portuguese and Moroccan coasts.

Using a specifically developed declustered catalog, [*Hamdache et al.*, 2016] computed various seismicity parameters in this region. The Atlas, considered as a whole, and the Moroccan Meseta demonstrate nearly identical values for the Gutenberg–Richter [*Gutenberg and Richter*, 1949] scaling b-value, but exhibit significantly different activity rates.

The Gutenberg–Richter recurrence relationship is defined by the equation

$$\log_{10} N\ (\geq m) = a - bm \quad M_{\max} \geq m \geq m_c$$

being $N(\geq m)$ the cumulative number of events with magnitude larger than or equal to m, and a and b positive parameters; a-value measures the seismicity activity level, i.e., the activity rate of the region.

The scaling b-value reflects the relationship between large and small magnitude earthquakes, a parameter used in seismic hazard assessments. The computed b-values for these two tectonic regions are 1.04 and 0.93, respectively, with activity rates for earthquakes above $M_w = 4.0$ (normalized to a 10-year interval and a square cell with a 100-km side) of 0.73 for the Atlas and 0.43 for the Moroccan Meseta areas, clearly indicating a difference in their seismic activities. Regarding the Rif, when considered as a whole, a somewhat lower b-value of 0.87 is obtained; however, it has a greater mean activity rate of 1.91. This suggests that the Rif is expected to experience stronger seismic activity and a higher proportion of large and small events in the Moroccan region.

In [*Peláez et al.*, 2018a,b] proposed a seismogenic model (Fig. 1) focused on seismic hazard assessments for the studied region. The zoning model was delineated by adjusting the seismogenic zones to the boundaries of the main tectonic domains, considering both the established characteristics of the tectonic structures and the recorded seismicity.

The delineation of the proposed model is then based mainly on the seismic activity distribution, the tectonics and the stress pattern. To do this, the predominant focal mechanism solution was initially computed for each zone using a stress field inversion approach. The proposed model include the zone T1, corresponding to the Tell seismogenic zone, the Rif seismogenic zone, divided into three parts (R1a, R1b and R2), as displayed on the Fig. 1, the Atlas seismogenic source zones, denoted as HA-MA, HA-AA and HA, the Moroccan Meseta and High-Plateaus (HP) seismogenic source zones, denoted in the current study by MM and MA-HP, the north Alboran seismogenic zones, named ALB1 and ALB2, and the Atlantic region seismogenic sources, named GC, GB and ATL. Since seismic hazards and risk scales with the zone's maximum possible earthquake magnitude, seismic threats can be assessed based on this parameter. Its estimation and various procedures are discussed in detail in a later section.

3. Simulation of the September 8, 2023, Earthquake

As mentioned above, the Extremum system has been used to evaluate the possible consequences of the 2023 Moroccan event. Generally, the system can model the impact of an earthquake in the first minutes after establishing the earthquake parameters and assist in making decisions regarding rescue and other emergency measures operations.

The Extremum system's mathematical models facilitate the determination of key parameters related to earthquake-induced losses [*Frolova et al.*, 2017; *Larionov and Frolova*, 2003; *Larionov et al.*, 2003; *Methodology...*, 2000]. These parameters include: the number of buildings and structures classified according to the MMSK-86 scale [*Shebalin et al.*, 1986] that have endured varying levels of damage during earthquakes of intensity I; the number of fatalities and injuries with different levels of impact, provided that the buildings involved have sustained a specific level of damage; and the resultant number of homeless individuals. The system's models can also be employed to estimate debris volume and its characteristics, the extent of damage to population centers, the areas where buildings have experienced different states of damage, the length of blocked roads, and the number of fires and incidents triggered along lifeline systems, among other factors. The mathematical expectation of social losses $M(N_j)$ that are sustained in the buildings of type j, taking into

account that the migration of residents during the daytime and night can be found for a population center via

$$M(N) = \sum_{j=1}^{n} \iint_{S_c} \int_{0}^{24} \int_{I_{\min}}^{I_{\max}} P_{C_j}(I) \cdot f(x,y,I) \cdot \Psi_j(x,y) \cdot \theta(t) dI dt dx dy, \quad (1)$$

where $I_{\min}$ and $I_{\max}$ are the maximum and minimum possible earthquake intensities; S_c is the area of the population center; n is the number of building types under consideration according to the MMSK-86 scale [*Shebalin et al.*, 1986]; $P_{C_j}(I)$ is the probability of fatalities and injuries, given that an earthquake with intensity has caused damage to buildings of type j; $\Psi_j(x,y)$ is the density of population distribution within the area of interest in buildings of type j; $f(x,y,I)$ is the density function of earthquake intensity probabilities within unit area with coordinates x, y; $\theta(t)$ is a function derived from a statistical analysis of data on population migration during 24 hours. In the case that the statistical data for any country or city is not available, the following average θ values are used for computations:

- From 11:00 PM to 7:00 AM, $\theta(t) = 1.0$,
- From 7:00 AM to 9:00 AM, $\theta(t) = 0.6$,
- From 9:00 AM to 6:00 PM, $\theta(t) = 0.7$,
- From 6:00 PM to 8:00 PM, $\theta(t) = 0.65$,
- From 8:00 PM to 11:00 PM, $\theta(t) = 0.9$.

The probability of residents being affected by an earthquake with intensity I, $P_{C_j}(I)$ is estimated by the relation

$$P_{C_j}(I) = \sum_{i=1}^{5} P_m(I) \cdot P(C_i|B_i),$$

where $P_{C_j}(I)$ is the probability of residents to be affected by an earthquake with intensity I; $P_{B_i}(I)$ is the probability of definite i damage state of buildings that would suffice to produce a given earthquake intensity; $P(C_j/B_i)$ is the probability of people to survive j level of impact, provided the building involved has survived damage state i. The computations are carried out for the various types of buildings and structures as classified according to the MMSK-86 scale [*Shebalin et al.*, 1986]: building types A (constructed from local materials); building types B (bricks, hewn stone, or concrete blocks); building types C (reinforced concrete, frame, large-panel, and log houses); building types E7, E8, E9 (earthquake-resistant buildings designed and constructed to endure earthquakes with intensities of 7, 8, and 9).

The system's databases and mathematical models are regularly updated to simulate shaking intensity, damage to buildings and structures, and the number of fatalities and injuries. The outputs of the system after applying the databases include the distribution of damage states for various types of buildings, classified according to the improved version of the Medvedev–Sponheuer–Karnik scale (MSK-64) [*Medvedev et al.*, 1964], currently known as the MMSK-86 scale [*Shebalin et al.*, 1986], for the entire affected area as well as individually for each settlement. Specifically, the expected numbers of fatalities and injuries (at different rates or levels) for the overall region and each population center, the estimated number of triggered secondary technological accidents at fire and chemical hazard sites in the affected area, along with the characteristics of highway blockages and the total length of blocked roadways.

In the Extremum system, data regarding event source parameters (magnitude, location, and focal depth) are input for the computation of probable macroseismic intensity, considering possible orientation and shape of the isoseismals, considered elliptical. The obtained values of macroseismic intensity are used to simulate damage for various building types classified according to the MMSK-86 scale: type A buildings (made from local materials), type B buildings (made of brick, hewn stone, or concrete blocks), type C buildings (made

of reinforced concrete, frame, large panels, and wood), and types E7, E8, E9 (designed and constructed to withstand earthquakes with macroseismic intensities of 7, 8, and 9).

To ensure comparability of vulnerability functions/damage matrices obtained from different samples, the classification of building types given in the MMSK-86 scale is correlated with the types of buildings of the European Macroseismic Scale [*European...*, 1998] (Table 1).

Table 1. Correlation of building types and vulnerability classes of the MMSK-86 and EMS-98 scales [*Frolova et al.*, 2014]

Description of building types according to EMS-98	Vulnerability class	
	EMS-98	MMSK-86
Rubble stone, field stone	A	A
Adobe (earth brick)	A	A
Simple stone	B	A
Massive stone	C	B
Unreinforced (bricks/concrete blocks)	B	B
Unreinforced (brick) with RC floors	C	B
Reinforced or confined	D	C
Reinforced without earthquake-resistant design (ERD)	C	C
Reinforced with a minimum level of ERD	D	E7
Reinforced with an average level of ERD	E	E8
Reinforced with a high level of ERD	F	E9
Timber structures	D	C–E7

The reliability of near real-time loss simulation significantly depends on the uncertainty in determining earthquake parameters by seismological agencies, as well as on regional peculiarities of the seismic intensity model and vulnerability functions for various elements at risk.

3.1. Input Data for Simulation

In our simulation, we used the parameters provided by the USGS. According to this agency, the coordinates of the epicenter were $\varphi = 31.058°$N; $\lambda = 8.385°$W. The discrepancy in the event location compared to other seismological agencies ranges from a minimum of 1.4 km to an average of 14 km (Fig. 3). Such values spread is comparable in area to such large cities as Fez or Marrakech. As a result of an incorrectly selected epicenter, the intensity value and, consequently, the estimation of damages for urbanized territories may be estimated incorrectly. Such discrepancies show the importance of selecting the proper epicenter, providing a more reliable estimation of damages.

Based on the understanding of the event's focal mechanism, we assumed that the isoseisms are ellipse-shaped with an azimuth of 255°, and an ellipse compression factor (the ratio of the major b and minor a axes of elliptical isoseismals of the highest intensity grades), $k = 1.5$. Again, according to the information provided by the USGS, we assumed that the earthquake's depth was 26 km.

To increase the accuracy of the loss simulation, the data on Morocco's building inventory was updated to include the default information in the Extremum system databases. According to [*El Hammoumi et al.*, 2015], in the settlements of Morocco, buildings are divided into 5 categories. These are a) villas, b) multi-story buildings with reinforced concrete structures, c) traditional 1–2-story Moroccan rubble stone buildings, d) modern Moroccan 2-story stone on cement mortar buildings, and d) illegal buildings built without applying building codes and, thus, are somewhat vulnerable. This information about building stock distribution was used to estimate the proportions of different building types

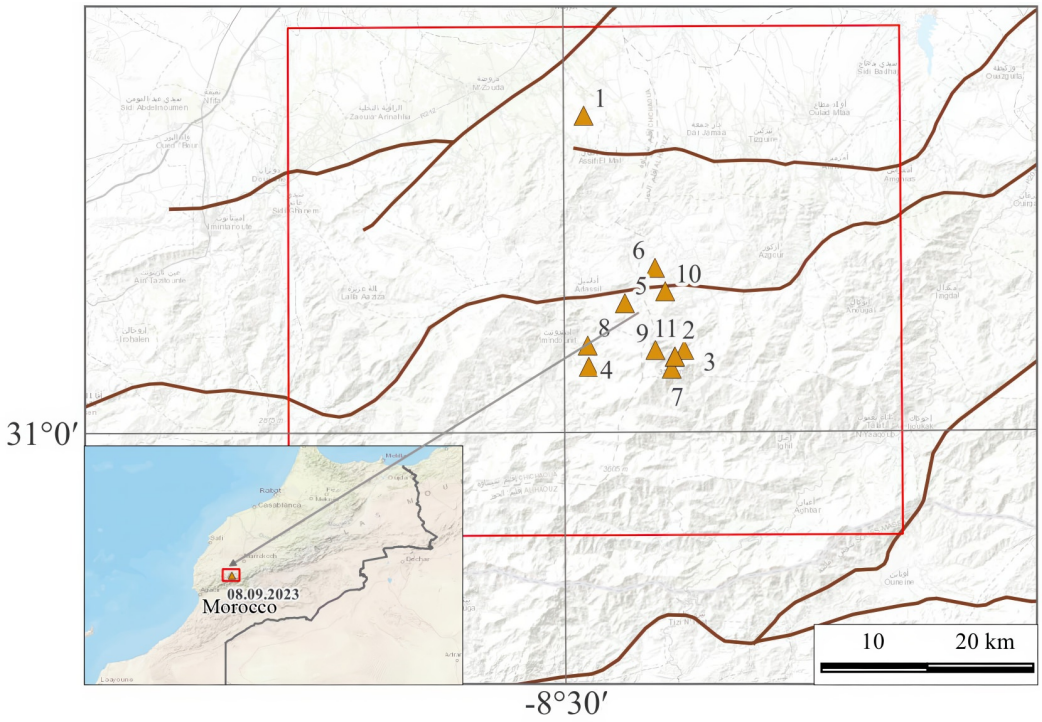

Figure 3. The September 8, 2023 epicenter according to the preliminary determination by: 1 – GS RAS, 2 – USGS, 3 – GDACS, 4 – EMSC, 5 – BGS, 6 – GEOPHON, 7 – INGV, 8 – NORSAR, 9 – Geoscience Australia, 10 – Seis. Survey Serbia, 11 – IRIS.

classified according to the seismic intensity scale MMSK-86 [*Shebalin et al.*, 1986]. Finally, two vulnerability functions/damage matrices according to [*Chavez et al.*, 1998] and those based on empirical data of the seismic intensity scale EMS-98 [*European...*, 1998] were used for damage assessment with the Extremum system application.

We used global and regional intensity prediction equations (IPEs) to simulate the macroseismic intensity. We initially applied the global IPEs [*New...*, 1982; *Shebalin et al.*, 1986] and [*Allen et al.*, 2012] proposed.

The global IPE by [*New...*, 1982; *Shebalin et al.*, 1986] is the following

$$\mathrm{I} = 1.5M - 3.5\log\sqrt{\Delta^2 + h^2} + 3 \tag{2}$$

being M the magnitude, I the seismic intensity at a distance Δ (km) from the epicenter, and h (km) the focal depth.

The relationship by Allen [*Allen and Wald*, 2009; *Allen et al.*, 2012] is the following:

$$I\left(\mathrm{M},\mathrm{R}_{\mathrm{hyp}}\right) = c_0 + c_1 M + c_2 \ln\sqrt{R_{\mathrm{hyp}}^2 + R_M^2} + S, \quad \text{for } R_{\mathrm{hyp}} \le 50\mathrm{km} \tag{3a}$$

$$I\left(\mathrm{M},\mathrm{R}_{\mathrm{hyp}}\right) = c_0 + c_1 M + c_2 \ln\sqrt{R_{\mathrm{hyp}}^2 + R_M^2} + c_4 \ln\left(\frac{R_{\mathrm{hyp}}}{50}\right) + S, \quad \text{for } R_{\mathrm{hyp}} \le 50\,\mathrm{km} \tag{3b}$$

Being $R_{\mathrm{hyp}} = \sqrt{\Delta^2 + h^2}$, $R_M = m_1 + m_2 e^{(M-5)}$, $c_0 = 2.085$, $c_1 = 1.428$, $c_2 = -1.402$, $c_4 = 0.078$, $m_1 = -0.209$, and $m_2 = 2.042$. S is the site factor introduced by equations in [Equations 4 and 5 in *Allen et al.*, 2012].

The used regional IPEs were those proposed by [*Benouar*, 1994] for Algeria and the Algerian Atlas Mountains, and [*Cherkaoui*, 1991] for the Moroccan Atlas Mountains. [*Cherkaoui*, 1991] relationship is as follows:

$$I = 1.4M - 1.3\ln\left(\sqrt{\Delta^2 + h^2}\right) - 0.0013\left(\sqrt{\Delta^2 + h^2}\right) + 0.99\ln(h) - 0.0013h + 0.29. \tag{4}$$

The relationship by [*Benouar*, 1994] for Algeria is the following:

$$I = 1.43M - 2.28\ln\left(\sqrt{\Delta^2 + h^2}\right) - 0.0004\left(\sqrt{\Delta^2 + h^2}\right) + 6.29. \quad (5)$$

The relationship by [*Benouar*, 1994] for the Algerian Atlas Mountains is as follows:

$$I = 1.48M - 2.05\ln\left(\sqrt{\Delta^2 + h^2}\right) - 0.00074\left(\sqrt{\Delta^2 + h^2}\right) + 5.16. \quad (6)$$

The parameters are those used in Eq. (2).

Considering that the areas in question are part of the same tectonic zone – the Alpine folding zone [*Gorshkov*, 1963b; *Meghraoui and the IGBP-601 working group*, 2016] – previous studies by [*Benouar*, 1994] and [*Ambraseys*, 1985] were used to test other IPEs for this zone. These include the [*Aliaj*, 1982] relationship for the Turkey territory:

$$I = 2.12M - 1.38\ln(\Delta + 7) - 2.72 \quad (7)$$

and the [*Shebalin et al.*, 1998] relationship for southeastern Europe

$$I = 1.5M - 4.5\lg\sqrt{\Delta^2 + h^2} + 4.5. \quad (8)$$

The parameters are those used in Eq. (2).

3.2. Results of the Morocco 2023 Earthquake Consequences Simulation

The results of the intensity simulation using global IPEs were compared with the observed intensity values from GDACS data (https://www.gdacs.org). Figs. 4 and 5 display the residuals for IPEs, Eqs. (2) and (3), against distance. The residuals are binned in 20-kilometre intervals, with the median residual plotted as grey points. The solid gray line represents the average value, while the dashed lines indicate the standard deviation of the residuals.

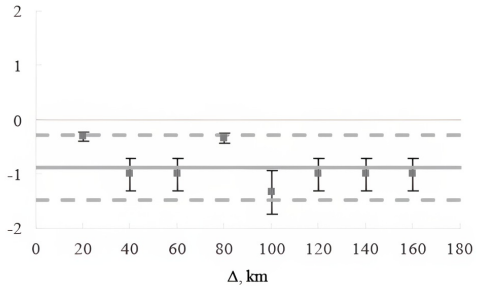

Figure 4. Residuals for calculated intensity according to IPE (Eq. (2)) against observed intensity values according to GDACS.

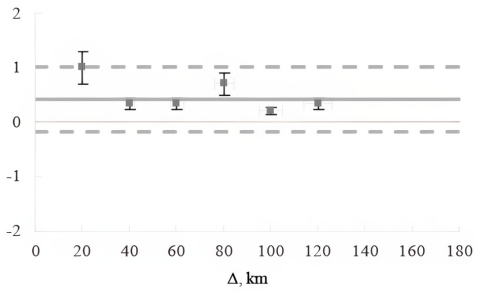

Figure 5. Residuals for calculated intensity according to IPE (Eq. (3)) against observed intensity values according to GDACS.

The [*New...*, 1982; *Shebalin*, 1968] global IPE appears to overestimate the calculated intensities against the observed ones for all epicentral distances (Fig. 4). Nevertheless, the Eq. (2) could be used in the nearest zone, for $\Delta < 20$ km. The [*Allen et al.*, 2012] global IPE fits the data at a distance range of 40 km $< \Delta <$ 120 km; on average, the residuals are less than 0.5 (Fig. 5).

Fig. 6 shows the simulation results with the application of IPEs from Eqs. (4) to (6) compared with observed values according to GDACS data.

The [*Cherkaoui*, 1991] relationship, IPE (Eq. (4)), for the High and Middle Atlas zones at a depth of 9.7 km, as determined by the author, performs well (Fig. 6a). When the [*Cherkaoui*, 1991] relationship is applied at a depth of 26 km (as provided by the USGS), the residuals reach 3 intensity degrees (Fig. 6b). The IPEs proposed by [*Benouar*, 1994] for

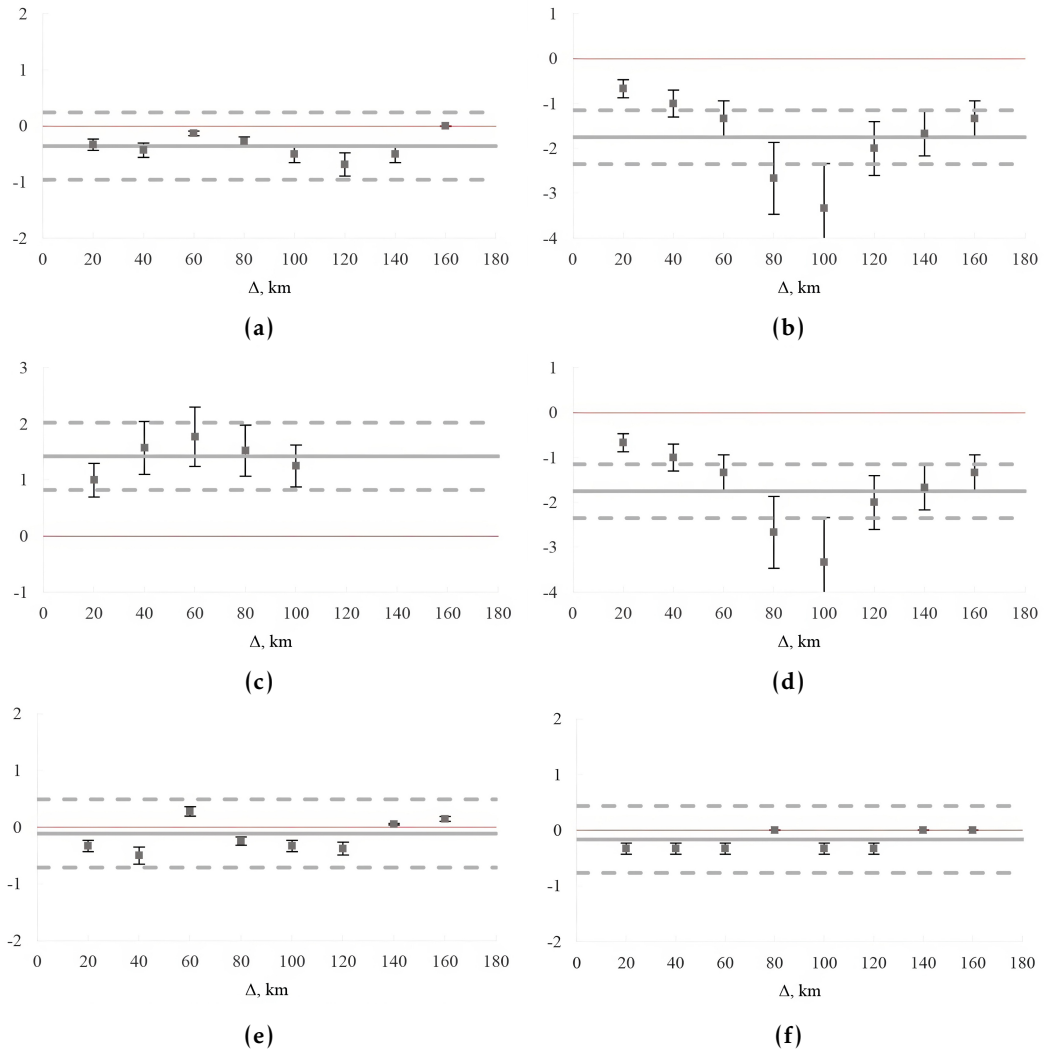

Figure 6. Residuals for calculated intensity according to IPEs Eqs. (4) to (6) versus distance according to GDACS data: (a) IPE (Eq. (4)), h = 9.7 km; (b) IPE (Eq. (4)), h = 26 km; (c) EPI (Eq. (5)), h = 6.8 km; (d) EPI (Eq. (5)), h = 26 km; (e) EPI (Eq. (6)), h = 4.8 km; (f) EPI (Eq. (6)), h = 26 km.

the Atlas Mountains (Eq. (4)) and for Algeria (Eq. (3)), across the various source depths considered, fit the available data well Figs. 6c to 6f. The residuals are close to zero for the studied range of distances.

Fig. 7 shows the residuals when using IPEs Eqs. (5) and (6), according to GDACS data, versus distance.

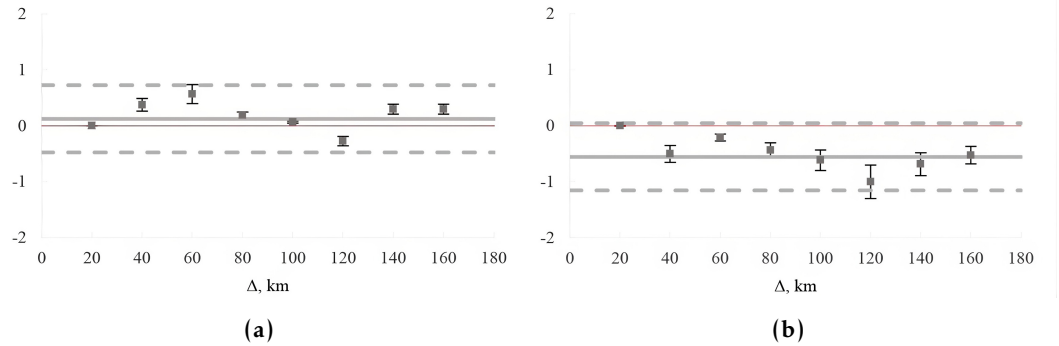

Figure 7. Residuals for calculated intensity according to the IPEs, Eqs. (5) and (6), according to GDACS data, versus distance: (a) IPE (Eq. (7)), h = 26 km; (b) IPE (Eq. (8)), h = 26 km.

Equation (5) regarding Turkey's territory [*Aliaj*, 1982] aligns well with the available data. The residuals are less than 0.5 intensity degrees (Fig. 7a). The application of the IPE (Eq. (8)) proposed by [*Shebalin et al.*, 1998] for southeastern Europe yields results similar to those obtained with Eq. (1), but on average, the difference between the observed and calculated values is negligible (Fig. 7b).

Initialy, the authors propose the IPEs Eqs. (4) to (6) for the average epicenter depth h_{av}. IPEs Eqs. (2), (4) and (8) use the USGS reported depth $h = 26$ km. Both depth estimations were used for computations. Table 2 presents the average difference between the calculated intensity and the observed ones according to GDASC for each intensity grade.

Table 2. Intensity residuals for the different IPEs

I, degree	Intensity Prediction Equations (IPEs)									
	1	2	3	3*	4	4*	5	5*	6	7
5	−0.9	0.2	−3.2	−0.8	−0.3	−0.3	−0.4	−0.4	−0.2	−0.9
6	−0.6	0.2	−2.7	−0.3	0.1	−0.1	−0.2	−0.3	0.3	−0.4
8	0.0	1.0	−1.8	0.0	0.0	−1.0	0.2	−1.0	0.7	0.2
average	−0.4	0.6	−2.5	−0.3	−0.1	−0.4	−0.1	−0.5	0.4	−0.3

* average depths h_{av}.

The analysis of Eqs. (3) to (6) and Table 2 allowed us to select the most suitable IPEs for simulating the Morocco 2023 earthquake. Fig. 8 shows the results of the simulation for IPE (Eq. (4)), with $h = 9.7$ km [*Cherkaoui*, 1991], for the High and Middle Atlas zone, and IPE (Eq. (5)), with $h = 26$ km [*Benouar*, 1994], for Algeria, which displayed a better alignment between the computed and observed intensities. The damage matrix according to EMS-98 was used for computation. Circles of varying sizes represent settlements with different populations; the circle's color indicates the average damage and the duration of construction within the settlements.

Figure 8 shows that the areas of the zones with average damage states $d_{av} = 3$, $d_{av} = 4$, and $d_{av} = 5$ are similar for IPEs (Eq. (4)) and (Eq. (5)).

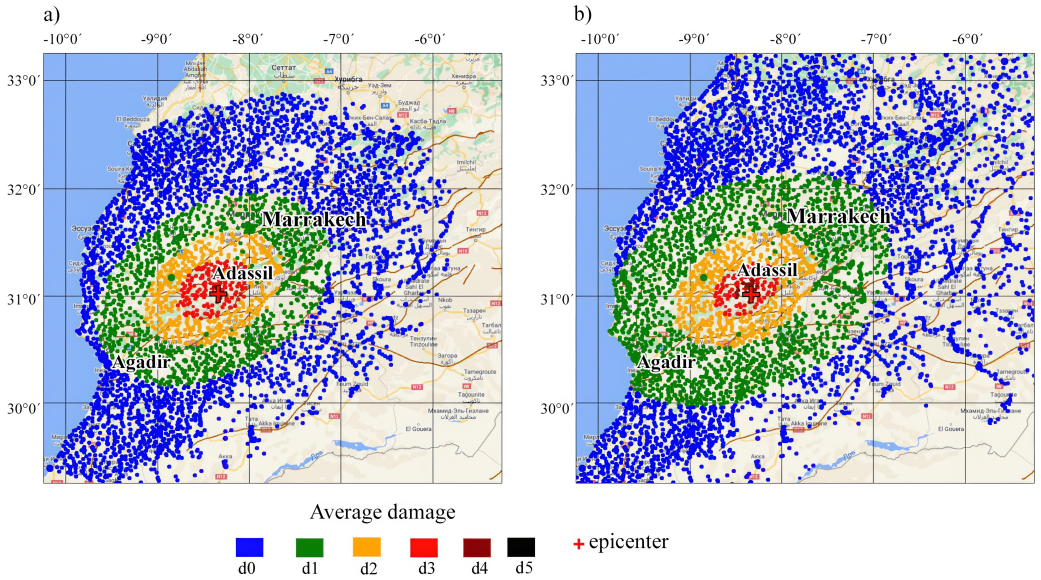

Figure 8. The September 8, 2023, earthquake simulation: (a) IPE (Eq. (5)), $h = 26$ km [*Benouar*, 1994]; (b) IPE (Eq. (4)), $h = 9.7$ km [*Cherkaoui*, 1991]. The EMS-98 damage matrix is used for simulation.

The information about settlements in the Extremum database was used to estimate the percentage of settlements that could experience different damage states d_{av} (Fig. 9). The probabilities of surviving by building stock severe damage states $d_{av} = 3$, $d_{av} = 4$, and $d_{av} = 5$ do not vary very much. It shows a relatively consistent response of the building stock to the experienced IPEs. At the same time, different IPEs significantly affect buildings'

probability of survival, for $d_{av} = 1$. It could be explained by the fact that the IPE (Eq. (4)) [*Cherkaoui*, 1991], with $h = 9.7$ km, overestimates the predicted intensity compared to the observed values within the range of intensity grades equal to $I = 5$ and less.

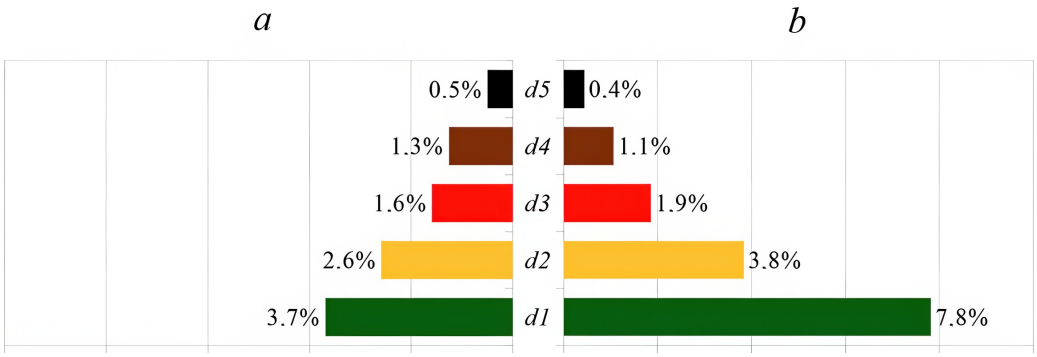

Figure 9. Percentage of settlements which survive different average damage states: (a) IPE (Eq. (5)), $h = 26$ km [*Benouar*, 1994]; (b) IPE (Eq. (4)), $h = 9.7$ km [*Cherkaoui*, 1991].

The IPE (Eq. (5)) with $h = 26$ km [*Benouar*, 1994] was used to assess the effects of applying different damage matrices: one by [*Chavez et al.*, 1998] and the EMS-98 [*European...*, 1998] (Fig. 10). Computations were performed for the four most affected settlements: Adassil, Targua, Imindounite, and Marrakech.

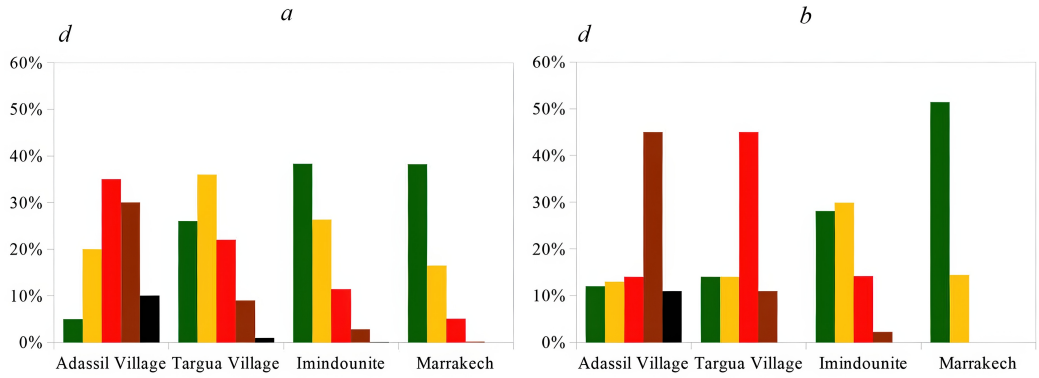

Figure 10. Distribution of building damage for some selected settlements with application of the IPE (Eq. (5)) [*Benouar*, 1994] for Algeria, $h = 26$ km: (a) damage matrix according to [*Chavez et al.*, 1998]; (b) damage matrix according to EMS-98 scale [*European...*, 1998]. Colors correspond to those used in Fig. 8.

Table 3 presents the estimated probabilities of separate damage states (d) and average damage states (d_{av}) for the building stock in Adassil, Targua, Imindounite, and Marrakech. Fig. 10 and Table 3 analysis indicate that the selected damage matrix influences the damage probability estimates. For instance, in the settlement of Imindounite, the estimated probability of building damage according to the two applied damage matrices for $d = 1$ differs by 27%. In the settlements of Marrakech and Imindounite, the difference in the probability of buildings surviving damage state ($d = 2$) is approximately 14%. For Adassil, the difference in estimating the probability of damage state ($d = 3$) reaches 60%.

It must also be mentioned that using a different damage matrix for simulation does not change the damage pattern. Namely, estimated average damage states for Adassil, Targua, Imindounite, and Marrakech settlements are similar. They vary from 1.4% for Imindounite and 8% for Marrakech.

A comparison of the damage estimates for the Adassil and Targua towns, located in the heavily affected province of Chichaoua (Figs. 11 to 12, United Nations Satellite Center, UNOSAT, [*UNOSAT*, 2023], shows a satisfactory agreement for damages stages $d_{av} = 4$ and $d_{av} = 5$.

Table 3. Simulated damage states d and d_{av} probabilities for some settlements for IPE (Eq. (3)), $h = 26$ km

Settlement	The probability of damage states determined by the damage matrix according to [*Chavez et al.*, 1998] and EMS 98					
	d_1	d_2	d_3	d_4	d_5	d_{av}
Adassil	0.05/0.12	0.20/0.13	0.35/0.14	0.30/0.45	0.10/0.11	3.20/3.15
Targua	0.26/0.14	0.36/0.14	0.22/0.45	0.09/0.11	0.01/0.0	2.05/2.21
Imindounite	0.38/0.28	0.26/0.30	0.11/0.14	0.03/0.02	0.0/0.0	1.37/1.39
Marrakech	0.38/0.51	0.16/0.14	0.05/0.0	0.0/0.0	0.0/0.0	0.87/0.80

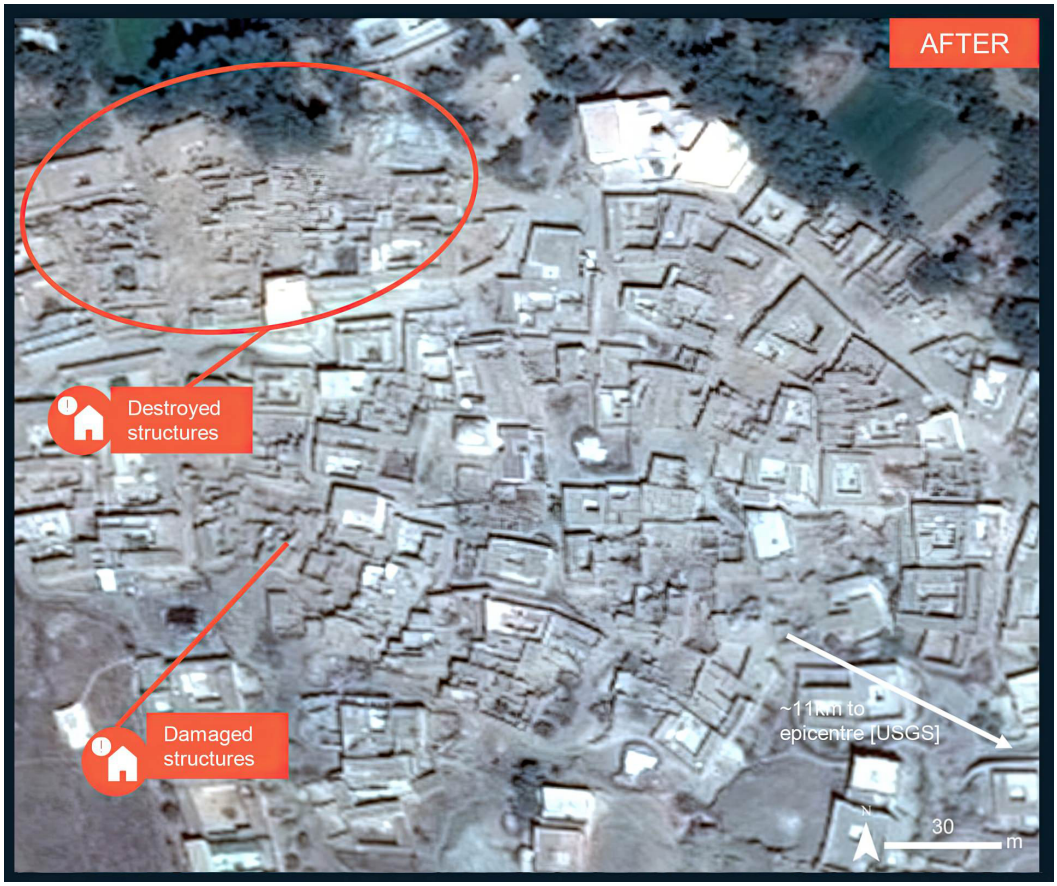

Figure 11. Observed damage in Adassil. Source: United Nations Satellite Center, UNOSAT, Preliminary Assessment Report [*UNOSAT*, 2023].

4. Regions With the Most Significant Seismic Hazard and Risk in Morocco and Its Surrounding Areas

So far, our investigation has focused on assessing the impact and effects of the M 6.8, 2023 Morocco earthquake. However, strong earthquakes also occur in other areas of the studied region [*Peláez et al.*, 2007] (Fig. 2). Therefore, it is reasonable to ask if we can briefly identify the areas exposed to the most significant seismic potential without applying the full formalism of seismic hazard assessment.

For engineering purposes, the maximum possible magnitude is defined as the upper limit of earthquake magnitude for a given region and is synonymous with the magnitude of the largest credible earthquake [*EERI Committee*, 1986; *WGCEP*, 1995]. The magnitude distribution assumes a sharp cutoff at this maximum magnitude; by definition, no earthquakes are expected to exceed this value. This definition contrasts with an alternative, 'soft' cutoff for maximum earthquake magnitude [*Kagan*, 1991, 2002a,b; *Pisarenko and Rodkin*, 2022], where one of the distribution parameters is referred to as the 'soft' maximum magnitude. Beyond this maximum magnitude, the distribution decays much faster than the

Figure 12. Observed damage in Targua. Source: United Nations Satellite Center, UNOSAT, Preliminary Assessment Report [*UNOSAT*, 2023].

classical Gutenberg–Richter relation. However, this implies that a 'soft' cutoff is envisaged, as earthquakes with magnitudes larger than this maximum magnitude are not excluded. Nonetheless, our work considers a model with only a sharp cutoff upper limit.

Assessing the upper limit of earthquake magnitude in a specific region is not straightforward. Thus, the upper limits of earthquake magnitudes for the seismogenic zones in these areas are examined using three distinct procedures: the weighted average of the three estimated values will be used as the solution. be considered. The three applied procedures are described in the following section.

5. Procedures for Assessing the Seismogenic Zones, Maximum Potential Earthquake Magnitude $M_{\max}$, and the Highest Earthquake Magnitude for the Seismogenic Zones of Morocco and Its Surroundings

Let us assume that in the area of concern, within a specified time interval T, all n of the main earthquakes that occurred with a magnitude greater than or equal to M_C, are recorded. The largest observed earthquake magnitude in the area is denoted as $m_{\max}^{\text{obs}}$. Next, assume that the value of the magnitude M_C is known and is denoted as the threshold of completeness. It is further assumed that the magnitudes are independent, identically distributed, random values with a probability density function (PDF), $f_M(m)$, and a cumulative distribution function (CDF), $F_M(m)$. The unknown parameter to be estimated, $m_{\max}$, is the upper limit of the range of magnitudes and is thus termed the maximum (seismogenic zone) earthquake magnitude $\hat{M}_{\max}$, which is to be estimated.

Let us assume further that the upper limit of earthquake magnitude $M_{\max}$ is estimated by the maximum likelihood method. Unfortunately, the sample likelihood function based on earthquake magnitudes [*Kijko and Sellevoll*, 1989, 1992] depends on the unknown $M_{\max}$.

This dependence violates the condition of regularity [*Cheng and Traylor*, 1995; *LeCam*, 1970]. The resulting likelihood function, therefore, reaches its maximum at the maximum observed earthquake magnitude $m_{\max}^{\text{obs}}$ and not at the required maximum *possible* magnitude $M_{\max}$. Consequently, the unbiased value of $M_{\max}$ cannot be estimated by using the standard maximum likelihood procedure. A more realistic and unbiased estimation of $M_{\max}$ can be provided by introducing additional information [*Pisarenko*, 1991; *Pisarenko et al.*, 2010], such as the condition that the largest observed earthquake magnitude $m_{\max}^{\text{obs}}$ within the span of the entire earthquake catalog, is equal to the largest *expected* earthquake magnitude $E\left[m_{\max}^{\text{obs}};t\right]$. In statistics, such an approach is known as the estimation-by-moment method [*Benjamin and Cornell*, 1970]. [*Kijko*, 2004] showed that the introduction of such a condition leads to the equation

$$M_{\max} = m_{\max}^{\text{obs}} + \int_{M_C}^{M_{\max}} [F|M(\zeta)]^n d\zeta, \tag{9}$$

being $F_M(\zeta)$ the CDF of earthquake magnitude limited from the top by the unknown $M_{\max}$.

The generic Eq. (9) is a basis for three $M_{\max}$ assessment procedures applied in our work: the parametric Kijko–Sellevoll Compound (K-S-C), the Non-Parametric-Gaussian (N-P-G) and the non-parametric Order Statistics (O-S) method. The procedures are based on the underlying principle that the estimated $M_{\max}$ value is equal to $m_{\max}^{\text{obs}} + \Delta$, where Δ a positive correction factor equal to $\int_{M_C}^{M_{\max}} [F|M(\zeta)]^n d\zeta$ (Eq. (9)). This principle is similar to the popular deterministic procedure, where the increment Δ varies from 1/4 to 1.0 of a magnitude unit [*Wheeler*, 2009]. Despite this similarity, there is a fundamental difference between the two approaches. In the deterministic approach, Wheeler's Δ is merely a guess. In the probabilistic approach, Δ is defined by parameters that characterize the area's seismicity; $m_{\max}^{\text{obs}}$, the seismic activity rate and the ratio between the number of weak and strong events. The correction factor relies on seismic parameters, aligning with the intuitive expectation that it is always positive, and its value diminishes as the observation time span increases. A brief description of each of the three procedures is provided below.

5.1. The Kijko-Sellevoll Compound Procedure (K-S-C)

Studies of seismic activity suggest that the seismic process can be composed of temporal trends, cycles, short-term oscillations and pure random fluctuations. When the variation of seismic activity is a random process, the formalism, in which the parameters of the earthquake recurrence model are treated as random variables, provides an efficient tool for modelling the seismic process [*Benjamin and Cornell*, 1970]. Following the assumption that a Gamma distribution can describe the variation of the scaling b-value in the frequency-magnitude Gutenberg–Richter relation [*Gutenberg and Richter*, 1942, 1956], it is possible to construct the compound estimator of $M_{\max}$. Following the generic Eq. (9), the estimation of $M_{\max}$ requires a calculation of the integral [*Kijko and Singh*, 2011]

$$\Delta = \left(C_\beta\right)^n \int_{M_C}^{M_{\max}} \left[1 - \left(\frac{p}{p + m - M_{\min}}\right)^q\right]^n dm,$$

which, after application of Cramer's approximation [*Cramer*, 1946], takes the form

$$\Delta = \delta^{\frac{1}{q}} \frac{\left[\exp\left(n\frac{r^q}{(1-r^q)}\right)\right]}{\beta}\left[\Gamma\left(\frac{-1}{q}, \delta r^q\right) - \Gamma\left(\frac{-1}{q}, \delta\right)\right],$$

where $\beta = b\ln(10)$, C_β is a normalizing coefficient equal to $\left[1 - \left(\frac{p}{p+m-M_C}\right)^q\right]^{-1}$, $p = \frac{\overline{\beta}}{(\sigma_\beta)^2}$ and $q = \left(\frac{\overline{\beta}}{\sigma_\beta}\right)^2$. The symbol $\overline{\beta}$ denotes the known mean value of the parameter β and σ_β is the known standard deviation of β, $r = \frac{p_\beta}{p_\beta + M_{\max} - M_C}$, $\delta = nC_\beta$, and $\Gamma(\cdot,\cdot)$ is the complementary

Incomplete Gamma Function [*Handbook...*, 1972]. Following Eq. (9), the compound version of the $M_{\max}$ estimator takes the form

$$M_{\max} = m_{\max}^{\text{obs}} + \frac{\delta^{\frac{1}{q}} \exp\left[\frac{nr^q}{(1-r^q)}\right]}{\overline{\beta}} \left[\Gamma\left(\frac{-1}{q}, \delta r^q\right) - \Gamma\left(\frac{-1}{q}, \delta\right)\right].$$

Since the unknown $M_{\max}$ is present on both sides of the equation in (9), the estimator for $M_{\max}$ can be calculated only through an iterative process. The approximate variance of the $M_{\max}$ estimator subsequently assumes the form

$$Var[M_{\max}] = \sigma_M^2 + \left[\frac{\delta^{\frac{1}{q}} \exp\left[\frac{nr^q}{(1-r^q)}\right]}{\overline{\beta}} \left[\Gamma\left(\frac{-1}{q}, \delta r^q\right) - \Gamma\left(\frac{-1}{q}, \delta\right)\right]\right]^2,$$

where σ_M denotes the standard error in the determination of the largest observed magnitude $m_{\max}^{\text{obs}}$.

5.2. Non-Parametric With Gaussian Kernel Procedure (N-P-G)

When the empirical distribution of earthquake magnitudes is complex and cannot be described by a simple analytical model, it can be replaced by its approximate non-parametric counterpart. Such a replacement can be done in several ways. This section shows how the earthquake magnitude distributions, both the probability density function (PDF) and cumulative distribution function (CDF), can be approximated by the sum of data-based kernel functions. Given the sample data m_i, $i = 1, \ldots, n$, and the kernel function $K(\cdot)$, the kernel estimator $\hat{f}_M(m)$ of an actual and unknown PDF $f_M(m)$,

$$\hat{f}_M(m) = \frac{1}{nh} \sum_{i=1}^{n} K\left(\frac{m - m_i}{h}\right),$$

where h is a positive smoothing factor [*Parzen*, 1962]. The kernel function is a PDF, symmetric about zero. The specific choice of it is not so crucial for the method's performance; many unimodal distribution functions ensure similar efficiencies. In this work, the Gaussian kernel function $K(\xi) = (2\pi)^{\frac{1}{2}} \exp(-\xi^2/2)$ is applied, where the smoothing factor h was estimated by the so-called least-squares cross-validation procedure [*Stone*, 1984]. [*Kijko et al.*, 2001] give the details of the applied approach.

Following the chosen kernel and the fact that the data comes from a finite interval $[M_C, M_{\max}]$, the respective CDF of seismic event magnitude takes the form

$$\hat{F}_M(m) = \begin{cases} 0, & \text{for } m < M_c \\ \dfrac{\sum_{i=1}^{n}\left[\Phi\left(\frac{m - m_i}{h}\right) - \Phi\left(\frac{M_c - m_i}{h}\right)\right]}{\sum_{i=1}^{n}\left[\Phi\left(\frac{M_{\max} - m_i}{h}\right) - \Phi\left(\frac{M_c - m_i}{h}\right)\right]}, & \text{for } M_c \le m \le M_{\max}, \\ 1, & \text{for } m > M_{\max} \end{cases}$$

where $\Phi(\xi)$ denotes the standard Gaussian cumulative distribution function. Therefore, following the generic Eq. (9), the estimator of $M_{\max}$ can be obtained through the iterative solution of the equation

$$M_{\max} = m_{\max}^{\text{obs}} + \Delta, \tag{10}$$

where

$$\Delta \cong \int_{M_c}^{M_{\max}} \left[\hat{F}_M(m)\right]^n dm = \int_{M_c}^{M_{\max}} \left[\frac{\sum_{i=1}^{n}\left(\Phi\left(\frac{m-m_i}{h}\right) - \Phi\left(\frac{M_c-m_i}{h}\right)\right)}{\sum_{i=1}^{n}\left(\Phi\left(\frac{M_{\max}-m_i}{h}\right) - \Phi\left(\frac{M_c-m_i}{h}\right)\right)}\right]^n dm. \tag{11}$$

So obtained the $M_{\max}$ value is denoted as the non-parametric Gaussian-based estimator of $M_{\max}$ or, in short, the N-P-G [*Kijko*, 2004] estimator. The approximate variance of the N-P-G estimator $\hat{M}_{\max}$ is given by

$$\mathrm{Var}\left(\hat{M}_{\max}\right) = \sigma_M^2 + \Delta^2,$$

where in Eq. (11), the upper limit of integration, $m_{\max}$, is replaced by its estimate $\hat{M}_{\max}$.

5.3. Procedure Based on Order Statistics

When the magnitude distribution's analytical form is unknown, it can be substituted by empirical distributions, and the formalism of the order statistics can be employed. For n earthquake magnitudes arranged in increasing order, i.e., $m_1 \le m_2 \le \ldots \le m_{n-1} \le m_n$, any empirical distribution function $\hat{F}_M(m)$ can be approximated as [*Cooke*, 1979]

$$\hat{F}_M(m) = \begin{cases} 0, & \text{for } m < m_1 \\ \dfrac{i}{n}, & \text{for } m_i \le m \le m_{i+1},\ i = 1,\ldots,n-1 \\ 1, & \text{for } m > m_n \end{cases}.$$

The approximate value of integral Δ is then [*Kijko and Singh*, 2011]

$$\Delta \equiv \int_{m_{\min}}^{m_{\max}^{\mathrm{obs}}} \left[\hat{F}_M(m)\right]^n dm = \sum_{i=1}^{n-1} \left(\frac{i}{n}\right)^n (m_{i+1} - m_i),$$

$$\Delta = m_{\max}^{\mathrm{obs}} - \sum_{i=0}^{n-1} \left[\left(1 - \frac{i}{n}\right)^n - \left(1 - \frac{i+1}{n}\right)^n\right] m_{n-i}.$$

Since for large n, the value of $(1 + 1/n)^n \cong e$, the correction factor $\Delta = m_{\max}^{\mathrm{obs}} - (1e^{-1}) \sum_{i=0}^{n-1} e^{-i} m_{n-i}$, and the order-statistics based estimator of $m_{\max}$ takes the form

$$\hat{M}_{\max} = m_{\max}^{\mathrm{obs}} + \left(m_{\max}^{\mathrm{obs}} - \left(1 - e^{-1}\right) \sum_{i=1}^{n-1} e^{-i} m_{n-i}\right). \tag{12}$$

In our work, the value of $M_{\max}$ obtained from Eq. (12) is denoted as the order statistics-based estimator or, in short, the O-S estimator. Assuming that the standard error in the determination of magnitude $m_1, \ldots, m_n$ is known and equal to σ_M, the approximate variance of the O-S estimator Eq. (12) is equal to

$$\mathrm{Var}(\hat{m}_{\max}) = c_0 \sigma_M^2 + \Delta^2, \tag{13}$$

where $c_0 = (1 + e^{-1})^2 + e^{-2}(1 - e^{-1})/(1 + e^{-1}) \cong 1.93$.

Both non-parametric estimators ((10), (11) and (12)) are very useful. The great attraction of the non-parametric approach is that it does not require specification of the functional form for the magnitude distribution $F_M(m)$. Therefore, by its nature, it can be applied to cases with empirical distributions of any complexity: distributions which considerably violate log-linearity, multimodality, and/or account for the presence of the 'characteristic' earthquakes. The drawback of the estimators is that formally they require knowledge of all events with magnitude above the specified level of completeness $m_{\min}$, though, in practice, this can be reduced to the knowledge of a few (e.g., only 5) of the largest events. Such a reduction is possible since the contribution of weak events to the correction factor Δ is insignificant.

5.4. The Maximum Earthquake Magnitude m_{max} for the Seismogenic Zones of Morocco and Its Vicinity

The data from the Spanish Instituto Geográfico Nacional (IGN) have been used to update the earthquake catalog compiled by [*Peláez et al.*, 2007] up to December 2023, to estimate the maximum possible magnitude for the previously described seismogenic source zone. The magnitudes of events have been converted to the moment magnitude scale using the same relations as [*Peláez et al.*, 2007]. Following the previously outlined procedures, the catalog for each seismogenic source zone has been removed from the updated dataset and utilised to determine the maximum possible magnitude. Table 4 display the results for the seismogenic zones considered in Morocco and its vicinity.

Table 4. Estimated maximum possible earthquake magnitudes and uncertainties for the considered seismogenic zones. The last column shows the weighted average of the three assessments of M_{max}, by the K-S-C, N-P-G, and O-S procedures

Zone	Time span of the catalog (years)	m_{max}^{obs} and second maximum magnitude	Estimated magnitude (non-parametric Gauss)	Estimated magnitude (non-parametric, based on order statistics)	Estimated magnitude (K-S-B)	Average (weighted)
T1	233	6.8/5.8	7.4 ± 0.6	7.2 ± 0.5	7.1 ± 0.3	7.18 ± 0.20
R2	978	6.6/6.0	6.9 ± 0.4	6.8 ± 0.4	6.8 ± 0.3	6.83 ± 0.21
R1a	201	6.0/5.2	6.5 ± 0.5	6.3 ± 0.4	6.4 ± 0.5	6.38 ± 0.26
R1b	232	6.3/6.2	6.5 ± 0.3	6.4 ± 0.3	6.5 ± 0.3	6.47 ± 0.17
MM	400	6.6/4.7	7.6 ± 1.0	7.3 ± 0.8	7.4 ± 1.4	7.41 ± 0.57
MA-HP	104	5.5/5.5	5.7 ± 0.3	5.6 ± 0.3	5.8 ± 0.3	5.70 ± 0.17
HA-MA	98	5.5/5.5	5.6 ± 0.2	5.6 ± 0.3	5.7 ± 0.3	5.62 ± 0.15
HA-AA	95	6.0/5.4	6.3 ± 0.4	6.3 ± 0.4	6.5 ± 0.5	6.35 ± 0.25
HA	90	6.8/5.8	7.4 ± 0.6	7.2 ± 0.5	7.8 ± 1.0	7.35 ± 0.36
GC	301	6.3/6.0	6.5 ± 0.3	6.5 ± 0.3	6.5 ± 0.3	6.50 ± 0.17
GB	667	7.8/7.1	8.4 ± 0.6	8.2 ± 0.5	8.4 ± 0.7	8.31 ± 0.34
ATL	105	5.5/5.4	5.6 ± 0.2	5.6 ± 0.3	5.7 ± 0.3	5.62 ± 0.15
ALB1	529	6.0/6.0	6.2 ± 0.3	6.1 ± 0.3	6.2 ± 0.3	6.17 ± 0.17
ALB2	531	6.3/6.3	6.4 ± 0.2	6.3 ± 0.3	6.3 ± 0.3	6.35 ± 0.15

It is important to note, as [*Kowsari et al.*, 2017] pointed out, that the largest observed magnitude, m_{max}^{obs} strongly influences the estimates of the maximum possible magnitude M_{max}. During the estimation of M_{max} (Table 4), the largest observed magnitude was assumed to occur within the catalog's duration. This is a significant assumption, and it may not be accurate. According to Kijko and Vermeulen [*Kijko and Vermeulen*, 2022], such an assumption can significantly impact the estimated values.

Additionally, seismic catalogs are often incomplete and inhomogeneous when considering historical data. As a result, the estimated earthquake recurrence parameters, including the scaling *b*-value of the Gutenberg–Richter recurrence relationship and the seismic activity rate, can be pretty uncertain. Consequently, among the three applied procedures, the non-parametric Gaussian (N-P-G) and order statistics (O-S) procedures provide more reliable estimates than the parametric K-S-C.

6. New Earthquake Scenario in the Moroccan Atlas Zone

The Extremum system was also used to evaluate the effects of two hypothetical earthquakes in the High Atlas region of Morocco. Based on assessments of M_{max} provided in Table 4, two events with magnitudes $M = 7.2$ and $M = 7.4$ were considered. Two IPEs, which demonstrated a relatively good agreement between the computed and observed

seismic intensities for the September 8, 2023, earthquake, were used in the computations. These include the IPEs by [*Cherkaoui*, 1991] with a focal depth of 9.7 km, and the IPEs by [*Benouar*, 1994], with a focal depth of 26 km.

The epicenter coordinates of the scenario events were taken according to NEIC for the earthquake occurred on September 08, 2023; specifically $\varphi = 31.064°$N; $\lambda = 8.391°$W. The depth was considered according to NEIC equal to $h = 26$ km and average depths h_{av} according to [*Cherkaoui*, 1991]. The coefficient $k = b/a$, representing the ratio of the large b and small a axis of the elliptical isoseismals of the highest intensity grades was taken $k = 1.5$. Additionally, the macroseismic field was oriented at 255° according to the fault-plane solution as determined by IRIS for the September 08, 2023 event, and the damage matrix according to [*Chavez et al.*, 1998] was applied.

Figs. 13 to 14 show the results of the simulated scenario $M_w = 7.2$ and $M_w = 7.4$ earthquakes, respectively, with consequences for magnitudes with the application of the IPEs (Eq. (2)) and (Eq. (3)).

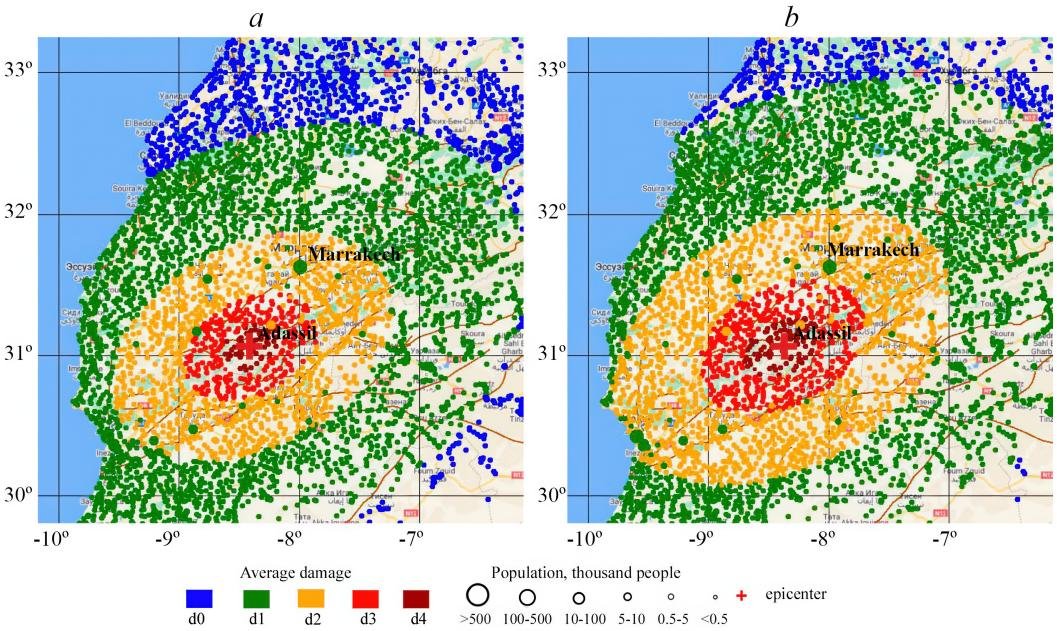

Figure 13. Scenario earthquake simulation consequences with application of IPE (Eq. (4)): (a) $M_w = 7.2$, (b) $M_w = 7.4$.

Table 5 shows the areas for the different isoseismals. Values for different magnitudes are shown in fraction.

Table 5. Areas for the different isoseismals (in %). In this case % is the area of the territory limited by isoseismals of the selected seismic intensity ranges to the total area of Morocco, which is taken to be equal to 446,550 km^2

I, grade	Areas limited by different isoseists (%)	
	IPE (Eq. (4)) $M_w7.2$ / $M_w7.4$	IPE (Eq. (5)) $M_w7.2$ / $M_w7.4$
$5I \le 6$	22.0/30.3	6.2/8.0
$6I \le 7$	6.3/9.1	2.7/3.4
$7I \le 8$	1.6/2.3	1.1/1.4
$8I \le 9$	0.4/0.6	0.5/0.6
$9I \le 10$	0.05/0.12	0.05/0.14

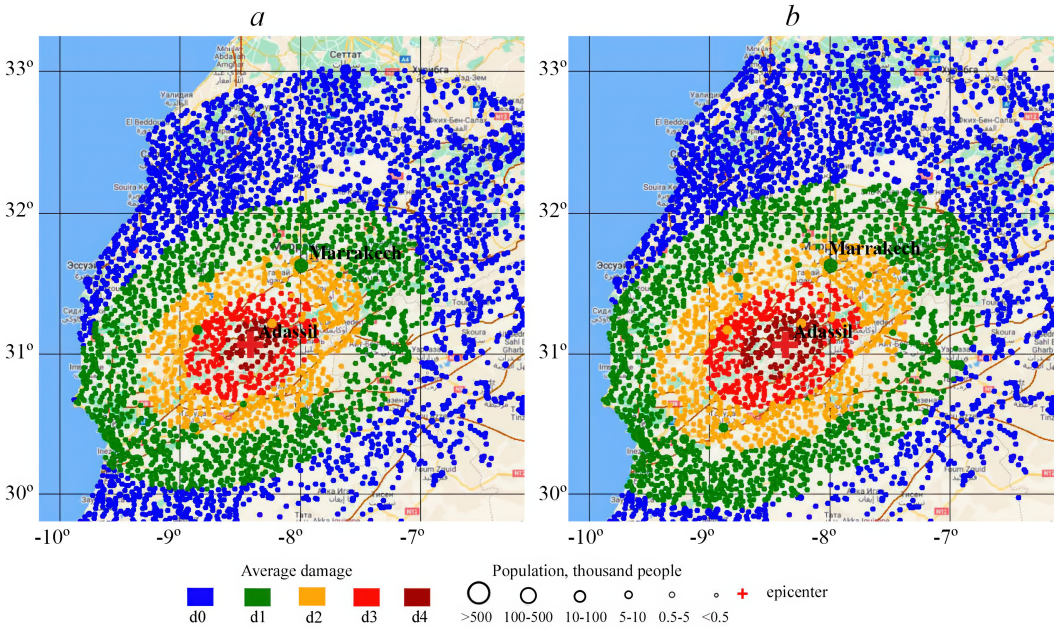

Figure 14. Scenario earthquake simulation consequences with application of IPE (Eq. (5)): (a) $M_w = 7.2$, (b) $M_w = 7.4$.

The strongest effect due to this scenario in the epicentral zone is obtained for IPE (Eq. (5)) ([*Benouar*, 1994]; Algeria, 26 km deep). But, the overall impact due to this scenario according due to IPE (Eq. (5)) is felt over a smaller area in comparison with IPE (Eq. (4)).

Table 6 shows the probabilities of different damage states d for settlements due to scenario events with magnitude equal to $M_w = 7.2$ and $M_w = 7.4$ and the damage matrix according to [*Chavez et al.*, 1998].

Table 6. Intensity residuals for the different IPEs

Settlement	I, grade	Probabilities of buildings damage states for scenario events with M_w7.2 / M_w7.4					
		$d = 1$	$d = 2$	$d = 3$	$d = 4$	$d = 5$	d_{av}
"village"	5–6	0.40	0.25	0.10	0.01	–	1 .24
	6–7	0.40–0.26	0.25–0.36	0.10–0.22	0.01–0.09	0.01	1.24–2.05
	7–8	0.26–0.05	0.36–0.20	0.22–0.35	0.09–0.30	0.01–0.10	2.05–3.2
	8–9	0.05–0.04	0.20–0.12	0.35–0.30	0.30–0.36	0.10–0.18	3.20–3.52
	9–10	0.04	0.12–0.05	0.30–0.12	0.36–0.13	0.18–0.70	3.52–4.48
"town"	5–6	0.39	0.16	0.05	–	–	0.86
	6–7	0.39–0.38	0.16–0.26	0.05–0.11	0.03	–	0.86–1.37
	7–8	0.38–0.26	0.26–0.31	0.11–0.22	0.03–0.11	0.02	1.37–2.07
	8–9	0.26–0.15	0.31–0.21	0.22–0.30	0.11–0.18	0.02–0.05	2.07–2.45
"city"	5–6	0.38	0.16	0.05	–	–	0.87
	6–7	0.38–0.36	0.16–0.27	0.05–0.12	0.03	–	0.87–1.40

Settlements, which are referred to the "village" class could survive damage states from $d_{av} = 1$ to $d_{av} = 4$. The building stock in "town" class settlements, less vulnerable, at large epicentral distances could survive damage states from $d_{av} = 1$ to $d_{av} = 3$. Built environment in the "city" class settlements could survive damage state equal to $d_{av} = 1$. This is due to the significant epicentral distance and the presence of buildings' types E7 (designed and constructed to withstand the earthquakes with intensity $I = 7$).

7. Summary and Conclusion

The primary goal of the present study is to evaluate the Extremum system in this region, using the data on the September 8, 2023, earthquake in Morocco, and then model the effect of the strongest earthquake that could occur in this region. The study takes into account the seismicity and seismoectonic features of the region where the September 8, 2023 earthquake struck.

An in-depth analysis has been performed looking into how the observed effects for the whole considered region and the seismically active Alpine-Himalayan belt differ from the intensities predicted by different IPEs. The process of calibrating the macroseismic field model of the Extremum system for the territory of Morocco was undertaken and the applicability of the IPEs obtained by researchers since 1960-th for the Upper and Middle Atlas zone, Algeria and the Atlas Mountains and the territory of Turkey was analyzed. The applicability of regional vulnerability functions of typical building stock for the reliable earthquake loss simulation outcomes was also investigated. The impact and effects of the September 8, 2023 (M_w = 6.8) Morocco earthquake have been assessed, however as mentioned previously, according to [*Peláez et al.*, 2007] strong earthquakes can also occur in other areas of the studied region. It should be noted that IPEs proposed by [*Cherkaoui*, 1991] for the High and Middle Atlas zone, and IPE [*Benouar*, 1994] for Algeria, give a better alignment between the computed and observed intensities.

The Extremum system was also used to evaluate the effects of two hypothetical earthquake scenarios in the High Atlas region of Morocco, with magnitude M_w = 7.2 and M_w = 7.4. These two earthquake scenarios have been obtained based on the assessment of the maximum possible magnitude of each zone-source of the proposed seismogenic source model by [*Peláez et al.*, 2018a,b].

Three distinct procedures were used to calculate the maximum magnitudes for these zones, and the weighted value is taken into account. The results of loss simulation due to scenario events in the most hazardous potential source zone in the High Atlas zone are given with application of the calibrated model of the macroseismic field of the Extremum system.

The relevance of the present study stems from the need for accurate estimates of potential losses resulting from recent earthquakes to support response decision-making, as well as from potential scenario events in the most hazardous zones to create and conduct early action plans intended to reduce seismic risk. The experience of search and rescue technician personnel after 6th February, 2023 earthquake in Turkey [*Polat*, 2024], as well as analysis of state of the art on Emergency management based on the peer-reviewed researches for 2018–2023 [*Sleiman et al.*, 2024] showed serious problems related to coordination and communication at every stage of disaster management, including lack of information on damage and casualties in emergency mode.

As the procedure for calibrating regional models of seismic intensity attenuation and regional vulnerability functions for typical building stock in the studied area involves identifying the boundaries of zones with quasi-stable field parameters and vulnerability functions, future efforts to clarify the calibrated field parameters and delineate the boundaries of zones for their application will require the collection of information on macroseismic manifestations of past events and their engineering consequences in the region under consideration. To successfully calibrate models of the Extremum system and other global systems used for near real-time assessments of earthquake consequences, it is essential to create and promptly replenish a knowledge base on the macroseismic and engineering-seismological effects of earthquakes. In this regard, international cooperation in the field of Big Data processing and the establishment of a distributed knowledge base on the physical and socio-economic impacts of past significant earthquakes, within the framework of the UN/CODATA projects that specify the boundaries of calibration zones, appears crucial.

Acknowledgments. The article was prepared as part of the State Task of the Sergeev Institute of Environmental Geosciences, Russian Academy of Sciences, focused on research work no. 122022400105–9 titled "Forecasting, Modeling, and Monitoring Endogenous and Exogenous Geological Processes to Reduce Their Negative Consequences"; research support from the Spanish Ministry of Science and Innovation through grant PID2022-136678NB-I00AEI/FEDER, UE was given.

References

AISE. The Agadir, Morocco earthquake February 29, 1960. — Committee of Structural Steel Producers of American Iron, Steel Institute, 1962.

Ait Brahim L., Chotin P., Hinaj S., et al. Paleostress evolution in the Moroccan African margin from Triassic to present // Tectonophysics. — 2002. — Vol. 357, no. 1–4. — P. 187–205. — https://doi.org/10.1016/s0040-1951(02)00368-2.

Aliaj Sh. Basic Seismotectonic Feautures of Albania // Earthquake Risk Reduction in the Balkan region. Working Group A, Seismology, Seismotectonics, Seismic Hazards and Earthquake Predictions, Final Report, A27-A32. — Athens : UNESCO, UNDRO, 1982.

Allen T. I. and Wald D. J. Evaluation of ground-motion modeling techniques for use in Global ShakeMap - A critique of instrumental ground-motion prediction equations, peak ground motion to macroseismic intensity conversions, and macroseismic intensity predictions in different tectonic settings. — U.S. Geological Survey Open-File Report 2009-1047, 2009. — 114 p.

Allen T. I., Wald D. J. and Worden C. B. Intensity attenuation for active crustal regions // Journal of Seismology. — 2012. — Vol. 16, no. 3. — P. 409–433. — https://doi.org/10.1007/s10950-012-9278-7.

Ambraseys N. N. Intensity-attenuation and magnitude-intensity relationships for northwest European earthquakes // Earthquake Engineering & Structural Dynamics. — 1985. — Vol. 13. — P. 733–788.

Benjamin J. R. and Cornell C. A. Probability, Statistics, and Decision for Civil Engineers. — New York : McGraw-Hill, 1970. — 712 p.

Benouar D. Magnitude-intensity and intensity-attenuation relationships for atlas region and Algerian earthquakes // Earthquake Engineering & Structural Dynamics. — 1994. — Vol. 23, no. 7. — P. 717–727. — https://doi.org/10.1002/eqe.4290230703.

Chalouan A., Gil A. J., Chabli A., et al. cGPS Record of Active Extension in Moroccan Meseta and Shortening in Atlasic Chains under the Eurasia-Nubia Convergence // Sensors. — 2023. — Vol. 23, no. 10. — https://doi.org/10.3390/s23104846.

Chavez J., Goula X., Roca A., et al. Preliminary risk assessment for Catalonia (Spain) // Proc. 11th European Conference on Earthquake Engineering, Paris, 6-11 September [CD-ROM]. — 1998.

Cheng R. C. H. and Traylor L. Non-regular maximum likelihood problems // Journal of the Royal Statistical Society Series B: Statistical Methodology. — 1995. — Vol. 57, no. 1. — P. 3–24. — https://doi.org/10.1111/j.2517-6161.1995.tb02013.x.

Cherkaoui T. E. M. Fichier des séismes du Maroc et des régions limitrophes: 1901-1984. — Rabat, Morocco : Institut Scientifique, 1988. — 158 p. — (In French).

Cherkaoui T. E. M. Contribution á l'étude de l'aléa sismique au Maroc. — Université Joseph-Fourier - Grenoble I, 1991. — (In French).

Cooke P. Statistical inference for bounds of random variables // Biometrika. — 1979. — Vol. 66, no. 2. — P. 367–374. — https://doi.org/10.1093/biomet/66.2.367.

Craig T. J., Jackson J. A., Priestley K., et al. Earthquake distribution patterns in Africa: their relationship to variations in lithospheric and geological structure, and their rheological implications // Geophysical Journal International. — 2011. — Vol. 185, no. 1. — P. 403–434. — https://doi.org/10.1111/j.1365-246x.2011.04950.x.

Cramer H. Mathematical Methods of Statistics. — Princeton : Princeton University Press, 1946. — P. 589.

De Groeve T. Global Disaster Alert and Coordination System: More Effective and Efficient Humanitarian Response // The 14th TIEMS Annual Conference 2007 Book of Proceedings. — Split (Croatia) : Hydrographic Institute of the Republic of Croatia, 2007. — P. 324–334.

De Groeve T., Annunziato A., Gadenz S., et al. Real-time Impact Estimation of Large Earthquakes Using USGS Shakemaps // Proceedings of the International Disaster and Risk Conference. — Davos (Switzerland) : IDRC International Disaster Risk Reduction Center, 2008.

Delvaux D. and Sperner B. New aspects of tectonic stress inversion with reference to the TENSOR program // Geological Society, London, Special Publications. — 2003. — Vol. 212, no. 1. — P. 75–100. — https://doi.org/10.1144/gsl.sp.2003.212.01.06.

DeMets C., Gordon R. G. and Argus D. F. Geologically current plate motions // Geophysical Journal International. — 2010. — Vol. 181, no. 1. — P. 1–80. — https://doi.org/10.1111/j.1365-246x.2009.04491.x.

EERI Committee. Glossary of terms for probabilistic seismic-risk and hazard analysis // Bulletin of the New Zealand Society for Earthquake Engineering. — 1986. — Vol. 19, no. 3. — P. 155–157. — https://doi.org/10.5459/bnzsee.19.3.155-157.

El Hammoumi A., Iben Brahim A., Birouk A., et al. Assessment of Seismic Vulnerability of Urban Buildings in Morocco // International Journal of Earthquake Engineering and Hazard Mitigation (IREHM). — 2015. — Vol. 3, no. 1. — P. 24–28.

European Microseismic Scale 1998. EMS-98 / ed. by G. Grünthal. — Centre Européen de Géodynamique et de Séismologie, 1998. — https://doi.org/10.2312/EMS-98.FULL.EN.

Frolova N. I., Larionov V. I., Bonnin J., et al. Loss caused by earthquakes: rapid estimates // Natural Hazards. — 2017. — Vol. 88, S1. — P. 63–80. — https://doi.org/10.1007/s11069-016-2653-x.

Frolova N. I., Larionov V. I., Bonnin J., et al. Seismic Risk Cartographic Visualization for Crisis Management // Geography, Environment, Sustainability. — 2014. — Vol. 7, no. 4. — P. 4–27. — https://doi.org/10.24057/2071-9388-2014-7-4-4-27.

Gorshkov G. P. On the seismicity of Africa // Byulleten Soveta po seysmologii AN SSSR. — Moscow, 1963a. — No. 13. — (In Russian).

Gorshkov G. P. The seismicity of Africa, Chapter 3 // A review of the natural resources of the African continent. — UNESCO, 1963b.

Gutenberg B. and Richter C. F. Earthquake magnitude, intensity, energy, and acceleration // Bulletin of the Seismological Society of America. — 1942. — Vol. 32, no. 3. — P. 163–191. — https://doi.org/10.1785/bssa0320030163.

Gutenberg B. and Richter C. F. Seismicity of the Earth and Associated Phenomena. — Princeton, New Jersey : Princeton University Press, 1949.

Gutenberg B. and Richter C. F. Earthquake magnitude, intensity, energy, and acceleration: (Second paper) // Bulletin of the Seismological Society of America. — 1956. — Vol. 46, no. 2. — P. 105–145. — https://doi.org/10.1785/bssa0460020105.

Hamdache M., Peláez J. A., Gospodinov D., et al. Stochastic Modeling of the Al Hoceima (Morocco) Aftershock Sequences of 1994, 2004 and 2016 // Applied Sciences. — 2022. — Vol. 12, no. 17. — https://doi.org/10.3390/app12178744.

Hamdache M., Peláez J. A., Kijko A., et al. Energetic and spatial characterization of seismicity in the Algeria-Morocco region // Natural Hazards. — 2016. — Vol. 86, S2. — P. 273–293. — https://doi.org/10.1007/s11069-016-2514-7.

Handbook of Mathematical Functions With Formulas, Graphs, and Mathematical Tables / ed. by M. Abramowitz and I. A. Stegun. — U.S. Department of Commerce, National Bureau of Standards, 1972. — 1082 p.

Hasterok D., Halpin J. A., Collins A. S., et al. New Maps of Global Geological Provinces and Tectonic Plates // Earth-Science Reviews. — 2022. — Vol. 231. — P. 104069. — https://doi.org/10.1016/j.earscirev.2022.104069.

Henares J., López Casado C., Sanz de Galdeano C., et al. Stress fields in the Iberian-Maghrebi region // Journal of Seismology. — 2003. — Vol. 7, no. 1. — P. 65–78. — https://doi.org/10.1023/a:1021294015027.

Kagan Y. Y. Seismic moment distribution // Geophysical Journal International. — 1991. — Vol. 106, no. 1. — P. 123–134. — https://doi.org/10.1111/j.1365-246x.1991.tb04606.x.

Kagan Y. Y. Seismic moment distribution revisited: I. Statistical results // Geophysical Journal International. — 2002a. — Vol. 148, no. 3. — P. 520–541. — https://doi.org/10.1046/j.1365-246x.2002.01594.x.

Kagan Y. Y. Seismic moment distribution revisited: II. Moment conservation principle // Geophysical Journal International. — 2002b. — Vol. 149, no. 3. — P. 731–754. — https://doi.org/10.1046/j.1365-246x.2002.01671.x.

Kariche J., Meghraoui M., Timoulali Y., et al. The Al Hoceima earthquake sequence of 1994, 2004 and 2016: Stress transfer and poroelasticity in the Rif and Alboran Sea region // Geophysical Journal International. — 2018. — Vol. 212, no. 1. — P. 42–53. — https://doi.org/10.1093/gji/ggx385.

Kijko A. Estimation of the Maximum Earthquake Magnitude, m max // Pure and Applied Geophysics. — 2004. — Vol. 161, no. 8. — P. 1655–1681. — https://doi.org/10.1007/s00024-004-2531-4.

Kijko A., Lasocki S. and Graham G. Non-parametric Seismic Hazard in Mines // Pure and Applied Geophysics. — 2001. — Vol. 158, no. 9. — P. 1655–1675. — https://doi.org/10.1007/pl00001238.

Kijko A. and Sellevoll M. A. Estimation of earthquake hazard parameters from incomplete data files. Part I. Utilization of extreme and complete catalogs with different threshold magnitudes // Bulletin of the Seismological Society of America. — 1989. — Vol. 79, no. 3. — P. 645–654. — https://doi.org/10.1785/bssa0790030645.

Kijko A. and Sellevoll M. A. Estimation of earthquake hazard parameters from incomplete data files. Part II. Incorporation of magnitude heterogeneity // Bulletin of the Seismological Society of America. — 1992. — Vol. 82, no. 1. — P. 120–134.

Kijko A. and Singh M. Statistical tools for maximum possible earthquake magnitude estimation // Acta Geophysica. — 2011. — Vol. 59, no. 4. — P. 674–700. — https://doi.org/10.2478/s11600-011-0012-6.

Kijko A. and Vermeulen P. J. On pitfalls in the estimation of the maximum m max // Preprint. — 2022.

Kowsari M., Halldorsson B., Jónsson S., et al. On maximum earthquake scenario of the Tjornes fracture zone, North Iceland for seismic hazard assessment // 16th World Conference on Earthquake. — Santiago, Chile, 2017.

Larionov V. and Frolova N. Peculiarities of seismic vulnerability estimations // Natural Hazards in Russia, volume 6: Natural Risks Assessment and Management. — Moscow : Publishing company "KRUK", 2003. — P. 120–131. — (In Russian).

Larionov V., Sushchev S., Ugarov A., et al. Seismic risk assessment with GIS-technology application // Natural Hazards in Russia, volume 6: Natural Risks Assessment and Management. — Moscow : Publishing company "KRUK", 2003. — P. 209–231. — (In Russian).

LeCam L. On the Assumptions Used to Prove Asymptotic Normality of Maximum Likelihood Estimates // The Annals of Mathematical Statistics. — 1970. — Vol. 41, no. 3. — P. 802–828. — https://doi.org/10.1214/aoms/1177696960.

Letamo Alemayehu, B Kavitha and TP Tezeswi. Seismicity pattern of African regions from 1964-2022: b-value and energy mapping approach // Geomatics, Natural Hazards and Risk. — 2023. — Vol. 14, no. 1. — P. 2197104. — https://doi.org/10.1080/19475705.2023.2197104.

López Casado C., Sanz de Galdeano C., Molina Palacios S., et al. The structure of the Alboran Sea: an interpretation from seismological and geological data // Tectonophysics. — 2001. — Vol. 338, no. 2. — P. 79–95. — https://doi.org/10.1016/s0040-1951(01)00059-2.

Medvedev S., Sponheuer W. and Kárník V. Neue seismische Skala // 7. Tagung der Europäischen Seismologischen Kommission vom 24.9. bis 30.9. 1962 in Jena, DDR. — De Gruyter, 1964. — P. 69–76. — https://doi.org/10.1515/9783112756430-019. — (In German).

Meghraoui M. and the IGBP-601 working group. The Seismotectonic Map of Africa // Episodes. — 2016. — Vol. 39, no. 1. — P. 9–18. — https://doi.org/10.18814/epiiugs/2016/v39i1/89232.

Methodology for predicting the consequences of earthquakes. — Moscow : VNII GOChS, Extreme Situations Research Center, Seismological Center of IGE RAS, 2000. — 27 p. — (In Russian).

Mezcua J. Catálogo general de isosistas de la Península Ibérica. — Madrid : Instituto Geográfico Nacional, 1982. — (In Spanish).

Mridekh A. Géodynamique des bassins méso-cénozoiques de l'offshore d'Agadir (Maroc sud occidental). Contribution á la connaissance de l'évolution atlasique d'un segment de la marge atlantique marocaine. PhD Thesis. — Kenitra, Morocco : Faculty of Sciences, 2002.

New Catalog of Strong Earthquakes in the U.S.S.R. from Ancient Times Through 1977 / ed. by N. V. Kondorskaya and N. V. Shebalin. — M. : World Data Center A for Solid Earth Geophysics, 1982. — 608 p.

Nievas C. I., Crowley H., Weatherill G., et al. Real-Time Loss Tools: Open-Source Software for Time- and State-Dependent Seismic Damage and Loss Calculations - Features and Application to the 2023 Türkiye-Syria Sequence // Seismica. — 2025. — Vol. 4, no. 1. — https://doi.org/10.26443/seismica.v4i1.1238.

Parzen E. On Estimation of a Probability Density Function and Mode // The Annals of Mathematical Statistics. — 1962. — Vol. 33, no. 3. — P. 1065–1076. — https://doi.org/10.1214/aoms/1177704472.

Pedrera A., Ruiz-Constán A., Galindo-Zaldívar J., et al. Is there an active subduction beneath the Gibraltar orogenic arc? Constraints from Pliocene to present-day stress field // Journal of Geodynamics. — 2011. — Vol. 52, no. 2. — P. 83–96. — https://doi.org/10.1016/j.jog.2010.12.003.

Peláez J. A., Chourak M., Tadili B. A., et al. A Catalog of Main Moroccan Earthquakes from 1045 to 2005 // Seismological Research Letters. — 2007. — Vol. 78, no. 6. — P. 614–621. — https://doi.org/10.1785/gssrl.78.6.614.

Peláez J. A., Henares J., Hamdache M., et al. A Seismogenic Zone Model for Seismic Hazard Studies in Northwestern Africa // Moment Tensor Solutions. — Springer International Publishing, 2018a. — P. 643–680. — https://doi.org/10.1007/978-3-319-77359-9_29.

Peláez J. A., Henares J., Hamdache M., et al. An Updated seismic model for Northwestern Africa // 16th European Conference on Earthquake Engineering. — Thessaloniki : EAEE, 2018b.

Pisarenko V. F. Statistical Evaluation of Maximum Possible Magnitud // Izvestiya Akademii Nauk SSSR. Fizika Zemli. — 1991. — No. 9. — P. 38–46. — (In Russian).

Pisarenko V. F. and Rodkin M. Approaches to Solving the Maximum Possible Earthquake Magnitude (Mmax) Problem // Surveys in Geophysics. — 2022. — Vol. 43, no. 2. — P. 561–595. — https://doi.org/10.1007/s10712-021-09673-1.

Pisarenko V. F., Sornette D. and Rodkin M. V. Distribution of maximum earthquake magnitudes in future time intervals: application to the seismicity of Japan (1923-2007) // Earth, Planets and Space. — 2010. — Vol. 62, no. 7. — P. 567–578. — https://doi.org/10.5047/eps.2010.06.003.

Polat T. Kahramanmaraş Merkezli Depremlerin Arama Kurtarma Teknisyenleri Tarafindan Değerlendirilmesi // Afet ve Risk Dergisi. — 2024. — Vol. 7, no. 2. — P. 329–340. — https://doi.org/10.35341/afet.1287897.

Rosas F. M., Duarte J. C., Neves M. C., et al. Thrust-wrench interference between major active faults in the Gulf of Cadiz (Africa-Eurasia plate boundary, offshore SW Iberia): Tectonic implications from coupled analog and numerical modeling // Tectonophysics. — 2012. — Vol. 548/549. — P. 1–21. — https://doi.org/10.1016/j.tecto.2012.04.013.

Sébrier M., Siame L., Zouine E. M., et al. Active tectonics in the Moroccan High Atlas // Comptes Rendus. Géoscience. — 2006. — Vol. 338, no. 1/2. — P. 65–79. — https://doi.org/10.1016/j.crte.2005.12.001.

Shebalin N. V. Methods of using engineering seismological data in seismic zoning // Seismic zoning of the USSR. — M. : Nauka, 1968. — P. 95–121. — (In Russian).

Shebalin N. V., Ershov I. A., Shestoperov G. S., et al. Improved version of the seismic intensity scale (MMSK-86) based on the MSK-64 and MCCCC-73 scales (final report). — Moscow : MCCCC, Institute of Physical Earth Sciences of the USSR Academy of Sciences, 1986. — (In Russian).

Shebalin N. V., Leydecker G., Mokrushina N. G., et al. Earthquake Catalogue for Central and South-eastern Europe 342 BC - 1990 AD. — Final Report to Contract ETNU - CT 93 - 0087, 1998.

Skobelev S. F., Hanon M., Klerkx J., et al. Active faults in Africa: a review // Tectonophysics. — 2004. — Vol. 380, no. 3/4. — P. 131–137. — https://doi.org/10.1016/j.tecto.2003.10.016.

Sleiman Ch., Thomas K., Gray J., et al. Emergency Management of Tomorrow Research: Landscape Assessment. A Summary Report of Peer-Reviewed Research in Emergency Management from 2018-2023. — U.S. Department of Homeland Security, 2024.

Sparacino F., Palano M., Peláez J. A., et al. Geodetic Deformation versus Seismic Crustal Moment-Rates: Insights from the Ibero-Maghrebian Region // Remote Sensing. — 2020. — Vol. 12, no. 6. — P. 952. — https://doi.org/10.3390/rs12060952.

Stone C. J. An Asymptotically Optimal Window Selection Rule for Kernel Density Estimates // The Annals of Statistics. — 1984. — Vol. 12, no. 4. — https://doi.org/10.1214/aos/1176346792.

The OpenQuake-engine User Manual. Global Earthquake Model (GEM) Open-Quake Manual for Engine version 3.0.0. — GEM, 2018. — 198 p.

UNOSAT. Preliminary satellite-derived damage assessment. Adassil/Al Haouz, 6.8M earthquake of 08-09-2023 (22:11 UTC) Chichaoua Province, Marrakech-Safi Region, Morocco. — UNITAR, 2023.

van der Woerd J., Dorbath C., Ousadou F., et al. The Al Hoceima Mw 6.4 earthquake of 24 February 2004 and its aftershocks sequence // Journal of Geodynamics. — 2014. — Vol. 77. — P. 89–109. — https://doi.org/10.1016/j.jog.2013.12.004.

Vázquez R., Macías J. L., Alcalá-Reygosa J., et al. Numerical modeling and hazard implications of landslides at the Ardillas Volcanic Dome (Tacaná Volcanic Complex, Mexico-Guatemala) // Natural Hazards. — 2022. — Vol. 113, no. 2. — P. 1305–1333. — https://doi.org/10.1007/s11069-022-05348-1.

WGCEP. Seismic hazards in southern California: Probable earthquakes, 1994 to 2024 // Bulletin of the Seismological Society of America. — 1995. — Vol. 85, no. 2. — P. 379–439. — https://doi.org/10.1785/BSSA0850020379.

Wheeler R. L. Methods of Mmax estimation east of the Rocky Mountains. — U.S. Geological Survey Open-File Report 2009-1018, 2009. — 44 p.